Atmos. Chem. Phys., 20, 10459–10475, 2020
https://doi.org/10.5194/acp-20-10459-2020

Atmospheric Chemistry and Physics
Open Access
EGU

Evolution of NO_3 reactivity during the oxidation of isoprene

Patrick Dewald[1], Jonathan M. Liebmann[1], Nils Friedrich[1], Justin Shenolikar[1], Jan Schuladen[1], Franz Rohrer[2], David Reimer[2], Ralf Tillmann[2], Anna Novelli[2], Changmin Cho[2], Kangming Xu[3], Rupert Holzinger[3], François Bernard[4,a], Li Zhou[4], Wahid Mellouki[4], Steven S. Brown[5,6], Hendrik Fuchs[2], Jos Lelieveld[1], and John N. Crowley[1]

[1]Atmospheric Chemistry Department, Max-Planck-Institut für Chemie, 55128 Mainz, Germany
[2]Institute of Energy and Climate Research, IEK-8: Troposphere, Forschungszentrum Jülich GmbH, 52428 Jülich, Germany
[3]Institute for Marine and Atmospheric Research, IMAU, Utrecht University, Utrecht, the Netherlands
[4]Institut de Combustion, Aérothermique, Réactivité et Environnement (ICARE), CNRS (UPR 3021)/OSUC, 1C Avenue de la Recherche Scientifique, 45071 Orléans CEDEX 2, France
[5]NOAA Chemical Sciences Laboratory, 325 Broadway, Boulder, CO 80305, USA
[6]Department of Chemistry, University of Colorado Boulder, Boulder, CO 80209, USA
[a]now at: Laboratoire de Physique et Chimie de l'Environnement et de l'Espace (LPC2E), Centre National de la Recherche Scientifique (CNRS), Université d'Orléans, Observatoire des Sciences de l'Univers en région Centre – Val de Loire (OSUC), Orléans, France

Correspondence: John N. Crowley (john.crowley@mpic.de)

Received: 16 April 2020 – Discussion started: 11 May 2020
Revised: 7 July 2020 – Accepted: 31 July 2020 – Published: 8 September 2020

Abstract. In a series of experiments in an atmospheric simulation chamber (SAPHIR,[1] Forschungszentrum Jülich, Germany), NO_3 reactivity (k^{NO_3}) resulting from the reaction of NO_3 with isoprene and stable trace gases formed as products was measured directly using a flow tube reactor coupled to a cavity ring-down spectrometer (FT-CRDS). The experiments were carried out in both dry and humid air with variation of the initial mixing ratios of ozone (50–100 ppbv), isoprene (3–22 ppbv) and NO_2 (5–30 ppbv). k^{NO_3} was in excellent agreement with values calculated from the isoprene mixing ratio and the rate coefficient for the reaction of NO_3 with isoprene. This result serves to confirm that the FT-CRDS returns accurate values of k^{NO_3} even at elevated NO_2 concentrations and to show that reactions of NO_3 with stable reaction products like non-radical organic nitrates do not contribute significantly to NO_3 reactivity during the oxidation of isoprene. A comparison of k^{NO_3} with NO_3 reactivities calculated from NO_3 mixing ratios and NO_3 production rates suggests that organic peroxy radicals and HO_2 account for $\sim 50\,\%$ of NO_3 losses. This contradicts predictions based on numerical simulations using the Master Chemical Mechanism (MCM version 3.3.1) unless the rate coefficient for reaction between NO_3 and isoprene-derived RO_2 is roughly doubled to $\sim 5 \times 10^{-12}$ cm^3 molecule^{-1} s^{-1}.

1 Introduction

The atmospheric oxidation of volatile organic compounds (VOCs) of both biogenic and anthropogenic origin has a great impact on tropospheric chemistry and global climate (Lelieveld et al., 2008). Isoprene is one of the major organic (non-methane) compounds that is released in the environment by vegetation and contributes $\sim 50\,\%$ to the overall emission of VOCs into the atmosphere (Guenther et al., 2012). The most important initiators of oxidation for biogenic VOCs in the atmosphere are hydroxyl radicals (OH), ozone (O_3) and nitrate radicals (NO_3) (Geyer et al., 2001; Atkinson and Arey, 2003; Lelieveld et al., 2016; Wennberg et al., 2018). Our focus in this study is on NO_3, which is formed via the sequential oxidation of NO by ozone (Reactions R1 and R2). During the daytime, NO_3 mixing ratios are very low, owing to its efficient reaction with NO (Reaction R6) and its rapid photolysis (Reactions R7 and R8). Generally, NO_3 is present in mixing ratios greater than a few

[1]Simulation of Atmospheric PHotochemistry In a large Reaction

parts per trillion by volume (pptv) only at night-time, when it can become the major oxidizing agent for VOCs including isoprene (Reaction R5). In forested regions, reactions with biogenic trace gases, however, can contribute significantly to the daytime reactivity of NO_3 (Liebmann et al., 2018a, b).

Moreover, NO_2, NO_3 and N_2O_5 exist in thermal equilibrium (Reactions R3 and R4) so that the heterogeneous loss of N_2O_5 (and NO_3) at surfaces (Reactions R9 and R10) impacts on the lifetime of NO_3 in the atmosphere (Martinez et al., 2000; Brown et al., 2003, 2006, 2009b; Crowley et al., 2010).

$$NO + O_3 \rightarrow NO_2 + O_2 \quad \text{(R1)}$$
$$NO_2 + O_3 \rightarrow NO_3 + O_2 \quad \text{(R2)}$$
$$NO_2 + NO_3 + M \rightarrow N_2O_5 + M \quad \text{(R3)}$$
$$N_2O_5 + M \rightarrow NO_2 + NO_3 + M \quad \text{(R4)}$$
$$NO_3 + \text{isoprene} \rightarrow \text{products (e.g. } RONO_2, RO_2) \quad \text{(R5)}$$
$$NO_3 + NO \rightarrow 2NO_2 \quad \text{(R6)}$$
$$NO_3 + h\nu \rightarrow NO + O_2 \quad \text{(R7)}$$
$$NO_3 + h\nu \rightarrow NO_2 + O \quad \text{(R8)}$$
$$N_2O_5 + \text{surface} \rightarrow \text{products (e.g. } HNO_3) \quad \text{(R9)}$$
$$NO_3 + \text{surface} \rightarrow \text{products (e.g. particle nitrate)} \quad \text{(R10)}$$
$$RONO_2 + \text{surface} \rightarrow \text{products (e.g. } HNO_3) \quad \text{(R11)}$$

Although isoprene is mainly emitted by vegetation at daytime (Sharkey and Yeh, 2001; Guenther et al., 2012), during which its main sink reaction is with the OH radical (Paulot et al., 2012), it accumulates in the nocturnal boundary layer (Warneke et al., 2004; Brown et al., 2009a) where reactions of NO_3 and O_3 determine its lifetime (Wayne et al., 1991; Brown and Stutz, 2012; Wennberg et al., 2018). The rate constant (at 298 K) for the reaction between isoprene and NO_3 is 6.5×10^{-13} cm^3 molecule^{-1} s^{-1}, which is several orders of magnitude larger than for the reaction with O_3 (1.28×10^{-17} cm^3 molecule^{-1} s^{-1}) (Atkinson et al., 2006; IUPAC, 2020) and thus compensating for the difference in mixing ratios of NO_3 (typically 1–100 pptv) and O_3 (typically 20–80 ppbv) (Edwards et al., 2017). NO_3 is often the most important nocturnal oxidant of biogenic VOCs (Mogensen et al., 2015), especially in remote, forested environments where it reacts almost exclusively with biogenic isoprene and terpenes (Ng et al., 2017; Liebmann et al., 2018a, b). The reaction between isoprene and NO_3 leads initially to the formation of nitro isoprene peroxy radicals (NISOPOO, e.g. $O_2NOCH_2C(CH_3)$=$CHCH_2OO$) that can either react with NO_3, forming mostly a nitro isoprene aldehyde (NC4CHO, e.g. $O_2NOCH_2C(CH_3)$=$CHCHO$) and methyl vinyl ketone (MVK) or react further with other organic peroxy (RO_2), or hydroperoxy (HO_2) radicals, forming nitrated carbonyls, peroxides and alcohols (Schwantes et al., 2015).

The organic nitrates formed ($RONO_2$) can deposit on particles (Reaction R11); therefore, the NO_3 + isoprene system contributes to the formation of secondary organic aerosol (SOA) (Rollins et al., 2009; Fry et al., 2018). Together with heterogeneous uptake of N_2O_5 or NO_3 on particle surfaces (Reactions R9 and R10), the build-up of SOA from isoprene oxidation products forms a significant pathway for removal of reactive nitrogen species (NO_x) from the gas phase; a detailed understanding of the reaction between isoprene and NO_3 is therefore crucial for assessing its impact on SOA formation and NO_x lifetimes.

In this study, the NO_3-induced oxidation of isoprene was examined in an environmental chamber equipped with a large suite of instruments, including a cavity ring-down spectrometer coupled to a flow tube reactor (FT-CRDS) for direct NO_3 reactivity measurement (Liebmann et al., 2017). The NO_3 lifetime in steady state (the inverse of its overall reactivity) has often been derived from NO_3 mixing ratios and production rates, with the latter depending on the mixing ratios of NO_2 and O_3 (Heintz et al., 1996; Geyer and Platt, 2002; Brown et al., 2004; Sobanski et al., 2016b). The steady-state approach works only if NO_3 is present at sufficiently high mixing ratios to be measured (generally not the case during daytime), breaks down to a varying extent if a steady state is not achieved (Brown et al., 2003; Sobanski et al., 2016b), and may be influenced by heterogeneous losses of NO_3 or N_2O_5 (Crowley et al., 2011; Phillips et al., 2016), which are difficult to constrain. Comparing the steady-state calculations with the FT-CRDS approach (which derives the NO_3 reactivity attributable exclusively to VOCs) can provide insight into the main contributions to NO_3 reactivity and its evolution as the reaction progresses. In the following, we present the results of direct NO_3 reactivity measurements in the SAPHIR (Simulation of Atmospheric PHotochemistry In a large Reaction) environmental chamber under controlled conditions and explore the contributions of isoprene, peroxy radicals and stable oxidation products to NO_3 reactivity over a period of several hours as the chemical system resulting from NO_3-induced oxidation of isoprene evolves.

2 Measurement and instrumentation

An intensive study of the NO_3 + isoprene system (NO3ISOP campaign) took place at the SAPHIR chamber of the Forschungszentrum Jülich over a 3-week period in August 2018. The aim of NO3ISOP was to improve our understanding of product formation in the reaction between NO_3 and isoprene as well as its impact on the formation of SOA. Depending on the conditions (high or low HO_2/RO_2, temperature, humidity, and daytime or night-time), a large variety of oxidation products, formed via different reaction paths, exist (Wennberg et al., 2018). During NO3ISOP, the impact of varying experimental conditions on the formation of gas-phase products as well as secondary organic aerosol formation and composition was explored within 22 different experiments (see Table 1). Typical conditions were close to those found in the atmosphere with 5 ppbv of NO_2, 50–100 ppbv of

O_3 and 3 ppbv of isoprene, or (when high product formation rates were required) NO_2 was raised to 25 ppbv and isoprene to 10 ppbv. The high O_3 mixing ratios in the chamber ensured that NO was not detectable (< 10 pptv) in the darkened chamber.

The first 11 experiments of NO3ISOP were dedicated to gas-phase chemistry; in the second part seed aerosol ($(NH_4)_2SO_4$) was added and the focus shifted to aerosol measurements. Due to a contamination event in the chamber, the experiment from the 7 August is not considered for further analysis. The SAPHIR chamber and the measurements and instruments that are relevant for the present analysis are described briefly below.

2.1 The SAPHIR chamber

The atmospheric simulation chamber SAPHIR has been described in detail on various occasions (Rohrer et al., 2005; Bossmeyer et al., 2006; Fuchs et al., 2010), and we present only a brief description of some important features here: the outdoor chamber consists of two layers of FEP (fluorinated ethylene propylene) foil defining a cylindrical shape with a volume of 270 m^3 and a surface area of 320 m^2. The chamber is operated at ambient temperature and its pressure is ~ 30 Pa above ambient level. A shutter system in the roof enables the chamber to be completely darkened or illuminated with natural sunlight. Two fans result in rapid (2 min) mixing of the gases in the chamber, which was flushed with synthetic air (obtained from mixing high-purity nitrogen and oxygen) at a rate of 250 $m^3\,h^{-1}$ for several hours between each experiment. Leakages and air consumption by instruments leads to a dilution rate of typically $1.4 \times 10^{-5}\,s^{-1}$. Coupling to a separate plant chamber enabled the introduction of plant emissions into the main chamber (Hohaus et al., 2016).

2.2 NO_3 reactivity measurements: FT-CRDS

The FT-CRDS instrument for directly measuring NO_3 reactivity (k^{NO_3}) has been described in detail (Liebmann et al., 2017) and only a brief summary is given here. NO_3 radicals are generated by sequential oxidation of NO with O_3 (Reactions R1 and R2) in a darkened, thermostated glass reactor at a pressure of 1.3 bar. The reactor surfaces are coated with Teflon (DuPont, FEPD 121) to reduce the loss of NO_3 and N_2O_5 at the surface during the ~ 5 min residence time. The gas mixture exiting the reactor (400 sccm) is heated to 140 °C before being mixed with either zero air or ambient air (at room temperature) and enters the FEP-coated flow tube where further NO_3 production (Reaction R2), equilibrium reaction with N_2O_5 (Reactions R3 and R4), and NO_3 loss via reactions with VOCs/NO (Reactions R5/R6) or with the reactor wall (Reaction R10) take place. NO_3 surviving the flow reactor after a residence time of 10.5 s is quantified by CRDS at a wavelength of 662 nm. The NO_3 reactivity is calculated from relative change in NO_3 concentration when mixed with zero air or ambient air. In order to remove a potential bias by ambient NO_3/N_2O_5, sampled air is passed through an uncoated 2 L glass flask (~ 60 s residence time) heated to 45 °C to favour N_2O_5 decomposition before reaching the flow tube. Ambient NO_3 (or other radicals, e.g. RO_2) is lost by its reaction with the glass walls. In addition to the reaction of interest (Reaction R5), Reactions (R2) to (R4) and (R10) affect the measured NO_3 concentration so that corrections via numerical simulation of this set of reactions are necessary to extract k^{NO_3} from the measured change in NO_3 concentration, necessitating accurate measurement of O_3, NO and especially NO_2 mixing ratios. For this reason, the experimental setup was equipped with a second cavity for the measurement of NO_2 at 405 nm as described recently (Liebmann et al., 2018b). In its current state the instrument's detection limit is $\sim 0.005\,s^{-1}$. By diluting highly reactive ambient air with synthetic air, ambient reactivities up to $45\,s^{-1}$ can be measured. The overall uncertainty in k^{NO_3} results from instability of the NO_3 source and the CRDS detection of NO_3 and NO_2 as well as uncertainty introduced by the numerical simulations. Under laboratory conditions, measurement errors result in an uncertainty of 16 %. The uncertainty associated with the numerical simulation was estimated by Liebmann et al. (2017), who used evaluated rate coefficients and associated uncertainties (IUPAC), to show that the uncertainty in k^{NO_3} is highly dependent on the ratio between the NO_2 mixing ratio and the measured reactivity. If a reactivity of $0.046\,s^{-1}$ (e.g. from 3 ppbv of isoprene) is measured at 5 ppbv of NO_2 (typical for this campaign), the correction derived from the simulation would contribute an uncertainty of 32 % to the resulting overall uncertainty of 36 %. For an experiment with 25 ppbv of NO_2 and 10 ppbv of isoprene, large uncertainties (> 100 %) are associated with the correction procedure as the NO_3 loss caused by reaction with NO_2 exceeds VOC-induced losses. Later we show that data obtained even under unfavourable conditions (high NO_2 mixing ratios) are in accord with isoprene measurements, which suggests that the recommended uncertainties in rate coefficients for Reactions (R3) and (R4) are overly conservative.

The sampled air was typically mixed with ~ 50 pptv of NO_3 radicals, and the reaction between NO_3 and RO_2 radicals generated in the flow tube (Reaction R5) represents a potential bias to the measurement of k^{NO_3}. In a typical experiment (e.g. 3 ppbv of isoprene), the reactivity of NO_3 towards isoprene is $0.046\,s^{-1}$. A simple calculation shows that a total of 20 pptv of RO_2 radicals has been formed after 10.5 s reaction between NO_3 and isoprene in the flow tube. Assuming a rate coefficient of $\sim 5 \times 10^{-12}\,cm^3\,molecule^{-1}\,s^{-1}$ for reaction between NO_3 and RO_2, we calculate a 5 % contribution of RO_2 radicals to NO_3 loss. In reality, this value represents a very conservative upper limit as RO_2 is present at lower concentrations throughout most of the flow tube, and its concentration will be significantly reduced by losses to the reactor wall and self-reaction. In our further analysis we therefore do not consider this reaction.

Table 1. Experimental conditions in the SAPHIR chamber during the NO3ISOP campaign.

Date	T (°C)	H_2O (%)	D/N	O_3 (ppbv)	NO_2 (ppbv)	Isoprene (ppbv)	Seed aerosol	Notes
31 July	25–35	0	N	90–120	1–5	0	–	
1 August	22–31	0	N	85–115	2–5	1.2	–	
2 August	23–38	0	N	85–120	2–5	2.5	–	
3 August	30–42	1.3–2.7	D → N	45–100	1–5	2.5	–	
6 August	20–44	1.4	N → D	40–110	1–6	3.2	–	
7 August	20–41	0.45–0.6	N	45–60	3–4.5	2.3	–	contamination
8 August	22–28	0	N	75–115	13–30	8	–	
9 August	20–27	0	N	65–115	6–2.5	3	–	CO and propene
10 August	17–28	0	N	40–65	3–5.5	1.8	–	
12 August	14–36	0	N → D	70–115	4–12	3	–	CO
13 August	28–24	0	N	75–110	12–23	6	–	
14 August	18–24	0	N	70–110	13–22	13	$(NH_4)_2SO_4$	reduced fan operation
15 August	20–28	1.3–2	N	80–115	8–21	9	$(NH_4)_2SO_4$	
16 August	20–28	1.6	N → D	80–115	2–5	3	$(NH_4)_2SO_4$	
17 August	18–26	1.2–1.7	N → D	0–400	0–17	0	–	isobutyl nitrate, calibration
18 August	14–31	1.3–1.4	N → D	80–110	2–5	3.5	$(NH_4)_2SO_4$	β-caryophyllene
19 August	16–31	0.07	N	0–110	0–20	3	$(NH_4)_2SO_4$	MVK, N_2O_5 as NO_2 source
20 August	20–26	1.2–19	N	85–130	3–5	6	$(NH_4)_2SO_4$	β-caryophyllene
21 August	20–30	1.5–1.9	N	55–130	2–5	4.5	$(NH_4)_2SO_4$	CO and propene
22 August	18–33	1.3–17	N	75–110	2.5–8.5	5	$(NH_4)_2SO_4$	plant emissions
23 August	18–31	1.5–2.2	N	45–100	3.5–5	4	$(NH_4)_2SO_4$	
24 August	17–23	1–1.6	N	85–110	2.3–5.5	22	NH_4HSO_4	β-caryophyllene

D/N denotes if the experiment was conducted with the chamber roof opened (D: daytime) or closed (N: night-time) and in which order a transition was done. Only maximum values of measured isoprene are listed.

2.3 VOC measurements: PTR-ToF-MS

During the NO3ISOP campaign, isoprene and other VOCs were measured by two different PTR-ToF-MS (proton transfer reaction time-of-flight mass spectrometer) instruments. The PTR-TOF1000 (IONICON Analytic GmbH) has a mass resolution $> 1500\,m/\Delta m$ and a limit of detection of < 10 ppt for a 1 min integration time. The instrumental background was determined every hour by pulling the sample air through a heated tube (350 °C) filled with a Pt catalyst for 10 min. Data processing was done using PTRwid (Holzinger, 2015), and the quantification and calibration was done once per day, following the procedure as described recently (Holzinger et al., 2019).

The Vocus PTR (Tofwerk AG and Aerodyne Research Inc.) features a newly designed focusing ion–molecule reactor, resulting in a resolving power of $12\,000\,m/\Delta m$ (Krechmer et al., 2018). Calibration was performed on an hourly basis for 5 min. The isoprene measurements of the two instruments agreed mostly within the uncertainties (14 %). An exemplary comparison between the two instruments of an isoprene measurement can be found in the Supplement (Fig. S1). For the evaluation of the experiment on the 2 August, only data from the PTR-TOF1000 were available. For all the other experiments of the campaign, isoprene and monoterpene mixing ratios were taken from the Vocus PTR, owing to its higher resolution and data coverage.

2.4 NO_3, N_2O_5, NO_2, NO, and O_3 measurements

The NO_3/N_2O_5 mixing ratios used for analysis are from a harmonized data set including the measurements from two CRDS instruments. Data availability, quality and consistency with the expected $NO_3/N_2O_5/NO_2$ equilibrium ratios were criteria for selecting which data set to use for each experiment. Both instruments measure NO_3 (and N_2O_5 after its thermal decomposition to NO_3 in a heated channel) using cavity ring-down spectroscopy at a wavelength of ~ 662 nm. The 5-channel device operated by the Max Planck Institute (MPI) additionally measured NO_2 and has been described recently in detail (Sobanski et al., 2016a). Its NO_3 channel has a limit of detection (LOD) of 1.5 pptv (total uncertainty of 25 %); the N_2O_5 channel has a LOD of 3.5 pptv (total uncertainty of 28 % for mixing ratios between 50 and 500 pptv). Air was subsampled from a bypass flow drawing ~ 40 SLPM through a 4 m length of 0.5 in. (inner diameter, i.d.) PFA (perfluoroalkoxy alkane) tubing from the chamber. Variation of the bypass flow rate was used to assess losses of NO_3 (< 10 %) in transport to the instrument, for which correction was applied. Air entering the instrument was passed through a Teflon membrane filter (Pall Corp., 47 mm, 0.2 µm pore), which was changed every 60 min. Corrections for loss

of NO_3 and N_2O_5 on the filter and inlet lines were carried out as described previously (Sobanski et al., 2016a).

The second CRDS was built by the NOAA Chemical Sciences Laboratory (Dubé et al., 2006; Fuchs et al., 2008, 2012; Wagner et al., 2011; Dorn et al., 2013) and operated by the Institut de Combustion, Aérothermique, Réactivité et Environnement (ICARE). During the NO3ISOP campaign, the NOAA-CRDS was positioned beneath the chamber, and air was sampled through an individual port in the floor. The sampling flow rate was 5.5–7 L min^{-1} through a Teflon FEP line (i.d. 1.5 mm, total length about 0.9 m) extending by about 50 cm (i.d. 4 mm) with 25 cm (i.d. 4 mm) in the chamber. A Teflon filter (25 µm thickness, 47 mm diameter, 1–2 µm pore size) was placed downstream of the inlet to remove aerosol particles and changed automatically at an interval of 1.5–2 h, depending on the conditions of the experiments, such as the amount of aerosol in the chamber. The instrument was operated with a noise equivalent 1σ detection limit of 0.25 and 0.9 pptv in 1 s for the NO_3 and N_2O_5 channels, respectively. The total uncertainties (1σ) of the NOAA-CRDS instrument were 25 % (NO_3) and −8 %/+11 % (N_2O_5).

NO_2 mixing ratios were taken from a harmonized data set combining the measurements of the 5-channel CRDS with that of the NO_3 reactivity setup as well as the NO_x measurement of a thermal dissociation CRDS setup (Thieser et al., 2016). The NO_x measurement could be considered a NO_2 measurement since during dark periods of the experiments NO would have been present at extremely low levels. The total uncertainty associated with the NO_2 mixing ratios is 9 %.

NO was measured with a LOD of 4 pptv via chemiluminescence (CL; Ridley et al., 1992) detection (ECO Physics, model TR780), and ozone was quantified with a LOD of 1 ppbv by ultraviolet absorption spectroscopy at 254 nm (Ansyco, ozone analyser 41M). Both instruments operate with an accuracy (1σ) of 5 %.

2.5 Box model

The results of the chamber experiments were analysed using a box model based on the oxidation of isoprene by NO_3, OH and O_3 as incorporated in the Master Chemical Mechanism (MCM), version 3.3.1 (Saunders et al., 2003; Jenkin et al., 2015). In this work, the analysis focusses on the fate of the NO_3 radical, so the oxidation of some minor products was omitted in order to reduce computation time. Moreover, the most recently recommended rate coefficient (IUPAC, 2020) for the reaction between NO_3 and isoprene ($k_5 = 2.95 \times 10^{-12} \exp(-450/T)$ cm^3 $molecule^{-1}$ s^{-1}) was used instead of the value found in the MCM v3.3.1, which is 6.8 % higher. Chamber-specific parameters such as temperature and pressure as well as the time of injection and amount of trace gases added (usually O_3, NO_2 and isoprene) were the only constraints to the model. The chamber dilution flow was implemented as first-order loss rates for all trace gases and wall loss rates for NO_3 or N_2O_5 were introduced (see Sect. 3.2). The numerical simulations were performed with FACSIMILE/CHEKMAT (release H010, date 28 April 1987, version 1) at 1 min time resolution (Curtis and Sweetenham, 1987). The chemical scheme used is listed in the Supplement (Table S1).

3 Results and discussion

An overview of the experimental conditions (e.g. isoprene, NO_3, NO_2 and O_3 mixing ratios) on each day of the campaign is given in Fig. 1. The temperature in the chamber was typically between 20 and 30 °C but increased up to 40 °C when the chamber was opened to sunlight. The relative humidity was close to 0 % during most of the experiments before 14 August. After this date, the experiments focussed on secondary organic aerosol formation and humidified air was used.

We divide the experiments into two broad categories according to the initial conditions: type 1 experiments were undertaken with NO_3 production from 5 ppbv of NO_2 and 100 ppbv of O_3. The addition of isoprene with mixing ratios of ∼ 3 ppbv resulted in NO_3 reactivities of around 0.05 s^{-1} at the time of injection. The NO_3 and N_2O_5 mixing ratios were typically of the order of several tens of parts per trillion by volume (pptv) in the presence of isoprene under dry conditions. During humid experiments (with seed aerosol), NO_3 mixing ratios were mostly below the LOD in the presence of isoprene, owing to increased uptake of NO_3/N_2O_5 on particles. An exceptionally large isoprene injection (∼ 20 ppbv) resulted in the maximum NO_3 reactivity of 0.4 s^{-1} on the 24 August. In type 2 experiments, higher NO_3 production rates were achieved by using 25 ppbv of NO_2 and 100 ppbv of O_3. In these experiments, with the goal of generating high concentrations of organic oxidation products, isoprene mixing ratios of 10 ppbv resulted in reactivities of ∼ 0.2 s^{-1} at the time of isoprene injection. Owing to high NO_3 production rates, several hundred parts per trillion of NO_3 and a few parts per billion of N_2O_5 were present in the chamber.

Figure 1 shows that once isoprene has been fully removed at the end of each experiment, the NO_3 reactivity tends towards its LOD of 0.005 s^{-1}, indicating that the evolution of the NO_3 reactivity is closely linked to the changing isoprene mixing ratio.

3.1 Comparison of k^{NO_3} with calculated reactivity based on measurements of VOCs

The VOC contribution to the NO_3 reactivity is the summed first-order loss rate coefficient attributed to all non-radical VOCs present in the chamber that can be transported to the FT-CRDS according to Eq. (1):

$$k^{NO_3} = \sum k_i [\mathrm{VOC}]_i, \quad (1)$$

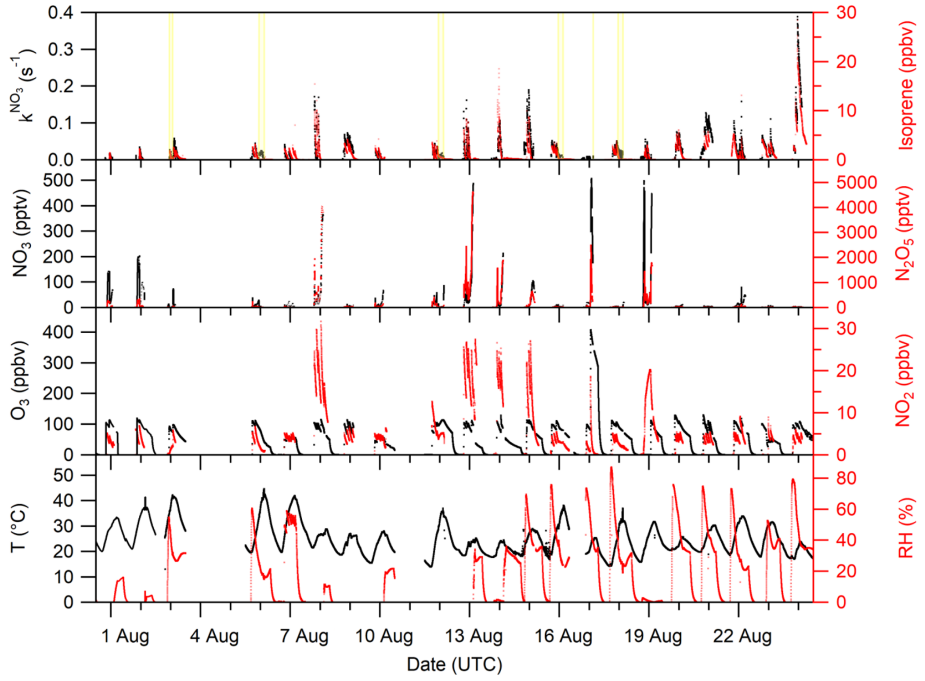

Figure 1. Overview of the temperature (T); relative humidity (RH); VOC-induced NO_3 reactivity (k^{NO_3}); and the O_3, NO_2, NO_3, N_2O_5, and isoprene mixing ratios during the NO3ISOP campaign. The yellow shaded area in the upper panel represent phases of the experiment when the chamber roof was opened. The ticks mark 12:00 UTC of the corresponding day.

where k_i is the rate coefficient (cm^3 $molecule^{-1}$ s^{-1}) for the reaction between a VOC of concentration $[VOC]_i$ and NO_3.

Reliable values of k^{NO_3} and VOC data are available from the 2 August onwards (see Table 1 for experimental conditions) and were used to compare FT-CRDS measurements of k^{NO_3} with $\Sigma k_i[VOC]_i$. For most of the experiments, isoprene was the only VOC initially present in the chamber, and at the beginning of the experiments k^{NO_3} should be given by k_5[isoprene], with the latter measured by the PTR-MS instruments (see above). On the 9 and 21 August, both isoprene and propene (100 ppbv) were injected into the chamber; the summed NO_3 reactivity from these trace gases was then k_5[isoprene] + $k_{propene}$[propene], with $k_{propene} = 9.5 \times 10^{-15}$ cm^3 $molecule^{-1}$ s^{-1} at 298 K (IUPAC, 2020). As no propene data were available, the propene mixing ratios were assessed with the model (see above) based on injected amounts as well as subsequent loss by oxidation chemistry (mainly ozonolysis) and dilution. On the 22 August, coupling to a plant emission chamber permitted the introduction of monoterpenes and isoprene into the main chamber so that the NO_3 reactivity was k_5[isoprene] + $k_{monoterpenes}$[monoterpenes]. The uncertainty in $\Sigma k_i[VOC]_i$ was propagated from the standard deviation of the isoprene and monoterpene mixing ratios and from the uncertainties of 41 % in k_5, 58 % in $k_{propene}$ (IUPAC, 2020) and 47 % in $k_{monoterpenes}$ (average uncertainty of three dominant terpenes; see below).

Figure 2a depicts an exemplary time series of k^{NO_3} and $\Sigma k_i[VOC]_i$ between the 9 and 13 August. The measured k^{NO_3} and values of $\Sigma k_i[VOC]_i$ calculated from measured isoprene (and modelled propene in the case of the 9 August) are, within experimental uncertainty, equivalent, indicating that the NO_3 reactivity can be attributed entirely to its reaction with isoprene (and other reactive trace gases like propene) injected into the chamber.

The correlation between k^{NO_3} and $\Sigma k_i[VOC]_i$ for the entire campaign data set is illustrated in Fig. 2b. Type 2 experiments (high NO_2 mixing ratios) were included despite the unfavourable conditions for measurement of k^{NO_3}, which result in large correction factors via numerical simulation (see above). The data points obtained on the 14 August display large variability, which is likely to have been caused by non-operation of the fans leading to poor mixing in the chamber. An unweighted linear regression of the whole data set yields a slope of 0.962 ± 0.003, indicating excellent agreement between the directly measured NO_3 and those calculated from Eq. (1). The intercept of (0.0023 ± 0.0004) s^{-1} is below the LOD of the reactivity measurement. A correlation coefficient of 0.95 underlines the linearity of the whole data set despite increased scatter caused by the unfavourable conditions during type 2 experiments. Note that data from the 7 August (chamber contamination) were not used. On the 15 and 21 August, additional flushing of the chamber with synthetic air (150–300 m^3) and humidification shortly before the actual beginning of the experiment resulted in a constant back-

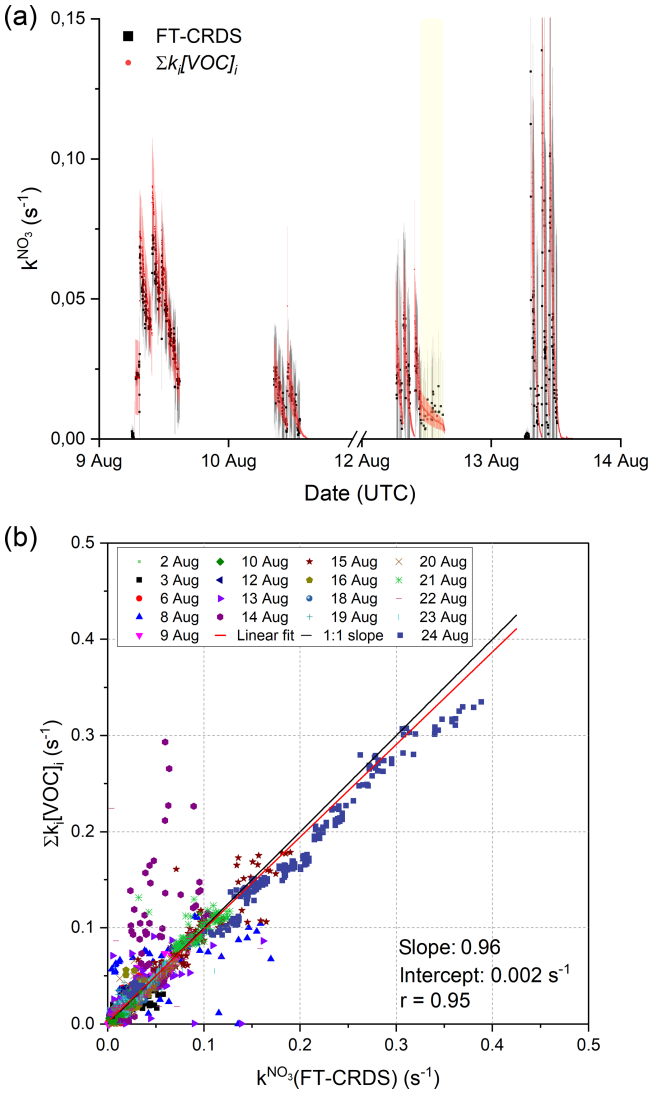

Figure 2. **(a)** 4 d time series of k^{NO_3} and $\Sigma k_i[\mathrm{VOC}]_i$. The total uncertainty in k^{NO_3} was calculated as described by Liebmann et al. (2017) and is indicated by the grey shaded area. The red shaded area shows the associated uncertainty of the calculated reactivities and are derived from error propagation using the standard deviation of the isoprene mixing ratios and an uncertainty of 41 % for the rate coefficient for reaction between NO_3 and isoprene (IUPAC, 2020). The ticks mark 00:00 UTC of the corresponding date, and yellow shaded areas represent periods in which the chamber roof was opened. **(b)** Correlation between $\Sigma k_i[\mathrm{VOC}]_i$ and k^{NO_3} measurements. The red line represents a least-squares linear fit to the entire data set, while the black line illustrates an ideal slope of 1 : 1.

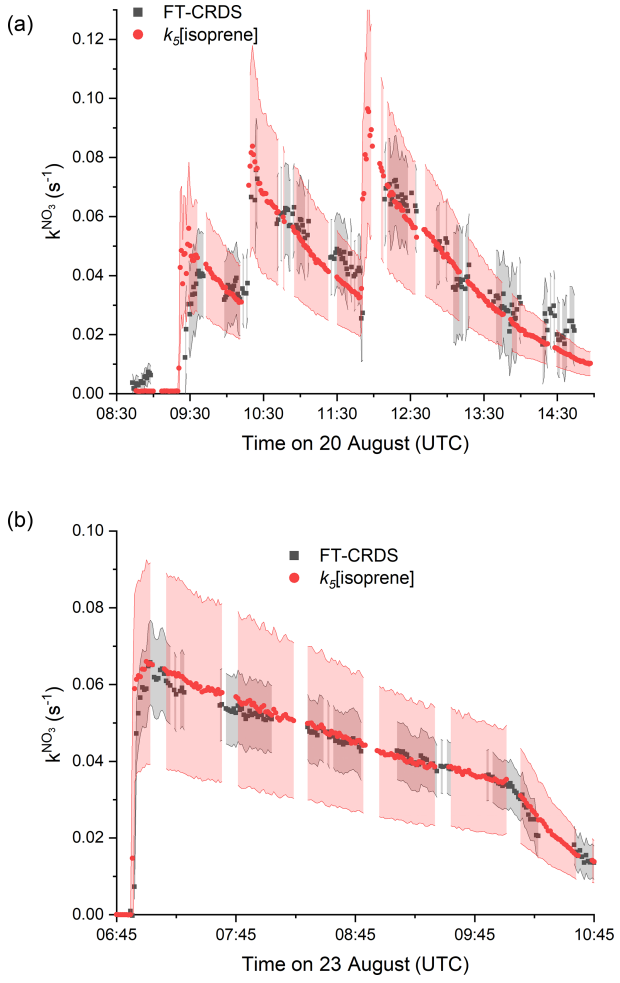

Figure 3. Measured reactivity (k^{NO_3}, black data points) and reactivity calculated from Eq. (1) (red data points), which is equivalent to k_5[isoprene]. The grey shaded area represents the total uncertainty in k^{NO_3}; the red shaded areas represent the total uncertainty in k_5[isoprene] and were estimated as explained in Fig. 2. **(a)** 20 August: type 1 experiment with initial mixing ratios of $NO_2 = 4.6$ ppbv and $O_3 = 120$ ppbv. **(b)** 23 August: only O_3 (100 ppbv) and isoprene (4 ppbv) were initially present.

ground reactivity in k^{NO_3} of 0.04 s^{-1} on the 15 August and 0.012 s^{-1} on the 21 August. High background reactivity was not observed during other humid experiments if the chamber was flushed extensively with synthetic air ($\sim 2000\ m^3$) during the night between experiments and if the additional flushing was omitted. The trace gas(es) causing this background reactivity could not be identified with the available measurements, but they are probably released from the chamber walls during flushing and humidification. In order to make a detailed comparison with the VOC data, the background reactivity, which was fairly constant, was simply added.

A more detailed examination of k^{NO_3} data from two type 1 experiments (low NO_2) is given in Fig. 3. The grey shaded areas indicate the total uncertainty associated with the FT-CRDS measurement of k^{NO_3} (Liebmann et al., 2017); the scatter in the data stems mostly from the correction procedure via numerical simulation.

On the 20 August (Fig. 3a), in addition to NO_2 and O_3, $(NH_4)_2SO_4$ seed aerosol ($\sim 50\ \mu g\ cm^{-3}$) and β-caryophyllene (~ 2 ppbv) were injected at 08:40 UTC in order to favour formation of secondary organic aerosol. The

instrument was zeroing until shortly after the injection of this terpene. As the lifetime of β-caryophyllene is extremely short in the chamber under the given conditions (~ 150 s), only the small fraction of unreacted β-caryophyllene contributes to the k^{NO_3} signal observed after 08:40 UTC. At 09:20, 10:13 and 11:50 UTC isoprene was injected into the chamber, resulting in step-like increases in the measured NO_3 reactivity. Each increase in reactivity and the ensuing evolution over time match well with the calculated values of k_5[isoprene] (red data points). The red shaded area indicates the overall uncertainty in the latter. Clearly, within experimental uncertainty, the NO_3 reactivity is driven almost entirely by reaction with isoprene, with negligible contribution from stable, secondary products.

During the experiment of the 23 August (Fig. 3b), only isoprene and ozone were present in the chamber for the first 4 h. Isoprene depletion is dominated by ozonolysis at this phase, whereas the sudden drop in k^{NO_3} is caused by an increased dilution flow during humidification of the chamber around 10:00 UTC. The absence of NO_2 results in a more accurate, less scattered measurement of k^{NO_3} and underscores the reliability of the measurement under favourable conditions. All of the observed reactivity can be assigned to isoprene that was injected at 06:52 UTC. This implies that stable secondary oxidation of products from isoprene ozonolysis (such as formaldehyde, MACR (methacrolein), MVK) are insignificant for k^{NO_3}, which is consistent with the low rate coefficients (e.g. $k_{MACR+NO_3} = 3.4 \times 10^{-15}$ cm^3 molecule^{-1} s^{-1} as highest of the three; IUPAC, 2020).

The results of a type 2 experiment with NO_2 mixing ratios of ~ 20 ppbv as well as higher isoprene mixing ratios (injections of ~ 8 and ~ 3 ppbv under dry conditions) are depicted in Fig. 4a. Despite the requirement of large correction factors to k^{NO_3} owing to the high NO_2 to isoprene ratios, fair agreement between measured k^{NO_3} and the expected reactivity is observed for each of the isoprene injections at 07:30, 09:20 and 10:50 UTC. The agreement may indicate that the uncertainty in k^{NO_3} (grey shaded area), which is based on uncertainty in, for example, the rate coefficient for reaction between NO_3 and NO_2 (Liebmann et al., 2017), is overestimated.

In Fig. 4b we display the results of an experiment on 12 August, in which the initially darkened chamber (first ~ 4 h) was opened to sunlight (final 4 h). NO_2 mixing ratios varied between 12 and 4 ppbv and isoprene was injected (~ 3 ppbv) three times at 05:55, 07:40 and 09:45 UTC. During the dark phase, measured k^{NO_3} follows k_5[isoprene]. At 11:00 UTC the chamber was opened to sunlight, during which approximately 5 ppbv of NO_2, 200–150 pptv of NO and < 1 ppbv of isoprene were present in the chamber. In this phase, the loss of NO_3 was dominated by its photolysis and reaction with NO. Within experimental uncertainty, the measured daytime k^{NO_3} after correction for both NO_2 and NO (correction factors between 0.05 and 0.02) during the sunlit period was still close to k_5[isoprene].

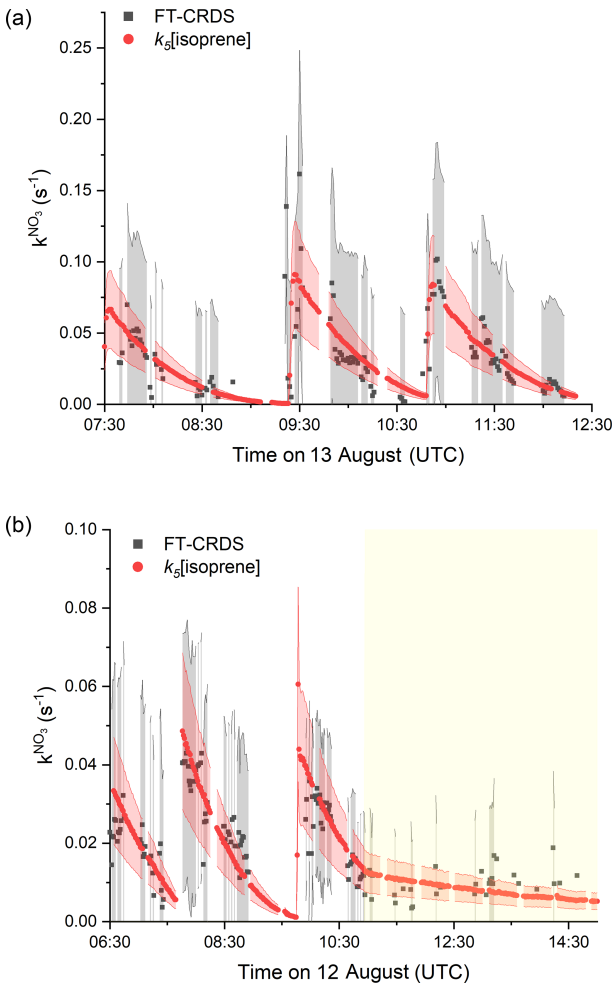

Figure 4. Measured (black) and expected (red) NO_3 reactivity using Eq. (1). The corresponding uncertainties were estimated as described in Fig. 2 and are indicated as shaded areas. **(a)** Type 2 experiment is from the 13 August under dry conditions with initial mixing ratios of $NO_2 = 25$ ppbv and $O_3 = 104$ ppbv. **(b)** Experiment from the 12 August is with NO_2 mixing ratios between 7 and 12 ppbv and initial mixing ratio of $O_3 = 79$ ppbv. The yellow shaded area denotes the period with the chamber roof opened after 11:00 UTC.

On the 22 August, the SAPHIR chamber was filled with air from a plant chamber (SAPHIR-PLUS) containing six European oaks (*Quercus robur*) which emit predominantly isoprene but also monoterpenes, mainly limonene, 3-carene and α-pinene (van Meeningen et al., 2016).

The time series of measured NO_3 reactivity (k^{NO_3}, black data points) after coupling to the plant chamber at 08:00 UTC is shown in Fig. 5. Data after 11:40 UTC are not considered, because the chamber lost its pressure after several recoupling attempts to the plant chamber. Also plotted (red data points) is the NO_3 reactivity calculated from $\Sigma k_i[\mathrm{VOC}]_i$, whereby both isoprene and the total terpene mixing ratio (up to 500 pptv) were measured by the Vocus PTR-MS. As only the mixing ratio of the sum of the monoterpenes

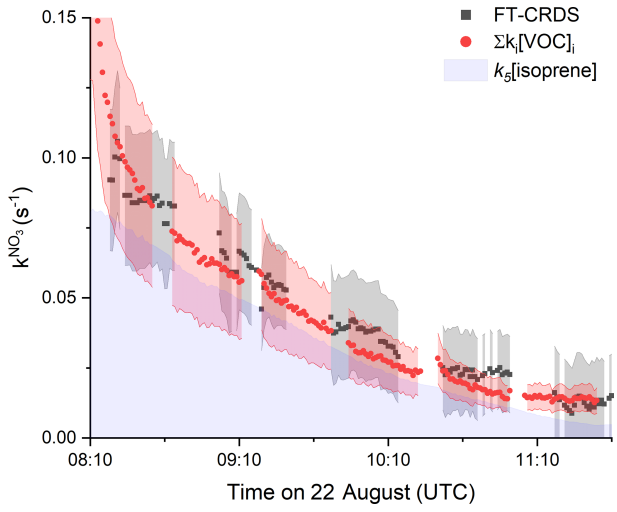

Figure 5. Results from 22 August between 08:00 and 11:40 UTC. Comparison between k^{NO_3} (black data points, uncertainty as grey shaded area) and NO_3 reactivity calculated from $\Sigma k_i[\mathrm{VOC}]_i$ (red data points) using the measured isoprene and Σmonoterpenes mixing ratios. The associated uncertainty (red area) was derived by error propagation by considering the standard deviations of the VOC mixing ratios as well as the uncertainties of the rate coefficients (41 % for k_5 and 47 % for $k_{\mathrm{monoterpenes}}$). The uncertainty of k^{NO_3} was estimated as explained in Fig. 2. The contribution of isoprene to the observed reactivity is indicated by the area in purple.

was known, an average value of the very similar NO_3 rate coefficients (IUPAC, 2020) for limonene, 3-carene and α-pinene was used for the calculation of $\Sigma k_i[\mathrm{VOC}]_i$ with $k_{\mathrm{monoterpenes}} = 9.1 \times 10^{-12}\,\mathrm{cm^3\,molecule^{-1}\,s^{-1}}$ (analogously averaged uncertainty of 47 %). Figure 5 indicates very good agreement between measured and calculated NO_3 reactivity, with ∼ 70 % of the overall reactivity caused by isoprene, which is indicated by the purple shaded area. Despite being present at much lower mixing ratios that isoprene, the terpenes contribute ∼ 30 % to the overall NO_3 reactivity, which reflects the large rate constants for reaction of NO_3 with terpenes.

The experiments described above indicate that, for a chemical system initially containing only isoprene as the reactive organic trace gas, the measured values of k^{NO_3} can be fully assigned to the isoprene present in the chamber over the course of its degradation. During the NO3ISOP campaign, not only NO_3 reactivity but also OH reactivity (k^{OH}) was measured; the experimental technique is described briefly in the Supplement. A detailed analysis of the OH reactivity data set will be subject of a further publication, and in Fig. S1 we only compare values of k^{NO_3} and k^{OH} obtained directly after isoprene injections, where k^{OH} should not be significantly influenced by the reaction of OH with secondary products. As shown in Fig. S2, isoprene concentrations derived from both k^{NO_3} and k^{OH} are generally in good agreement when [isoprene] < 5 ppbv.

The oxidation of isoprene by NO_3 in air results in the formation of stable (non-radical) products as well as organic peroxy radicals (RO_2) that can also react with NO_3. As radicals (e.g. NO_3, RO_2 and HO_2) are not sampled by the FT-CRDS, the equivalence of k^{NO_3} and k_5[isoprene] indicates that non-radical, secondary oxidation products do not contribute significantly to the NO_3 reactivity.

3.2 Steady-state and model calculations: role of RO_2 and chamber walls

The contribution of RO_2, HO_2 and stable products to NO_3 reactivity was examined using a box model based on the chemical mechanistic oxidation processes of isoprene by NO_3, OH and O_3 as incorporated in the Master Chemical Mechanism, version 3.3.1 (Saunders et al., 2003; Jenkin et al., 2015; Khan et al., 2015). A numerical simulation (Fig. 6) of the evolution of NO_3 reactivity was initialized using the experimental conditions of the first isoprene injection on 10 August (5.5 ppbv NO_2, 60 ppbv O_3 and 2 ppbv isoprene, dry air), including chamber-specific parameters such as temperature, the NO_3 and N_2O_5 wall loss rates (quantified in detail below), and the dilution rate. In the model, NO_3 reacts with both stable products and peroxy radicals. One of several major stable oxidation products according to MCM is an organic nitrate with aldehyde functionality ($O_2NOC_4H_6CHO$, NC4CHO). As the corresponding rate coefficient for the reaction of this molecule with NO_3 is not known, MCM uses a generic rate coefficient based on the IUPAC-recommended temperature-dependent expression for acetaldehyde + NO_3 scaled with a factor of 4.25 to take differences in molecular structure into account. The maximum modelled mixing ratio of NC4CHO was ∼ 5 ppbv in type 2 experiments, which would result in a NO_3 reactivity of 0.001 $\mathrm{s^{-1}}$. This value is below the instrument's LOD and would only become observable at extremely low isoprene concentrations. As apparent in Fig. 6, the contribution of stable oxidation products (blue) to the NO_3 reactivity is insignificant compared to the primary oxidation of isoprene (red).

Since the rate coefficients for reaction of isoprene-derived peroxy radicals and NO_3 are (unlike NO_3+HO_2) poorly constrained by experimental data, the MCM uses a generic value of $2.3 \times 10^{-12}\,\mathrm{cm^3\,molecule^{-1}\,s^{-1}}$, which is based on the rate coefficient for the reaction between NO_3 and $C_2H_5O_2$. The modelled overall NO_3 reactivity when reactions with RO_2 and HO_2 are included (black line) is on average 22 % higher than the reactivity associated only with isoprene, with the major contributors to the additional NO_3 reactivity being nitrooxy isopropyl peroxy radicals ($O_2NOC_5H_8O_2$, NISOPOO) formed in the primary oxidation step. As neither RO_2 nor HO_2 radicals will survive the inlet tubing (and heated glass flask) between the SAPHIR chamber and the FT-CRDS instrument, our measurement of k^{NO_3} does not include their contribution. The measured values of k^{NO_3} (black data points) scatter around the isoprene-induced reactivity

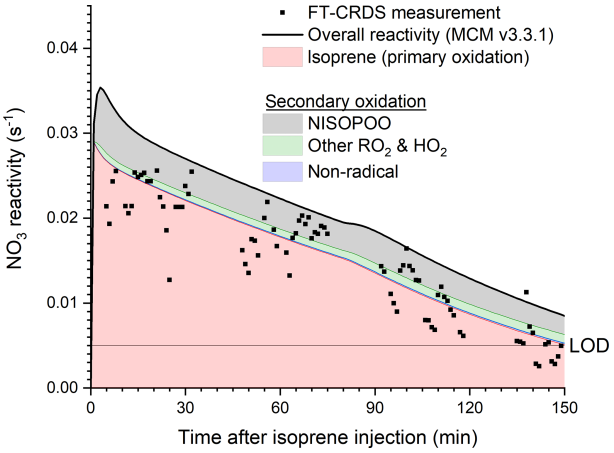

Figure 6. Experimental results for k^{NO_3} and numerical simulation (MCM v3.3.1) of the NO_3 reactivity following the first isoprene injection of the experiment on the 10 August. The simulation was run with 1 min resolution; initial conditions were 60 ppbv of O_3, 5.5 ppbv of NO_2 and 2 ppbv of isoprene and used actual chamber temperatures, which increased from 293 to 301 K during the course of the experiment. Wall losses of NO_3 and N_2O_5 were parameterized as described in the text. Individual contributions to the NO_3 reactivity of isoprene, peroxy radicals and secondary oxidation products are highlighted.

(red), which is understood to result from the minor role of stable (non-radical) oxidation products (blue) in removing NO_3 and the exclusion of peroxy radicals in the measurement.

Another method of deriving NO_3 reactivity is to calculate it from NO_3 (and/or N_2O_5) mixing ratios and production rates under the assumption of steady state as has been carried out on several occasions for the analysis of ambient NO_3 measurements (Heintz et al., 1996; Geyer and Platt, 2002; Brown et al., 2004; Sobanski et al., 2016b). In contrast to our direct measurement of k^{NO_3}, all loss processes (including reaction of NO_3 with RO_2 and HO_2 and uptake of NO_3 and N_2O_5 to surfaces) are assessed using the steady-state calculations. A comparison between k^{NO_3} and NO_3 reactivity based on a steady-state analysis should enable us to extract the contribution of peroxy radicals and wall losses of NO_3 in the SAPHIR chamber. In steady state, the NO_3 reactivity ($k_{ss}^{NO_3}$) is derived from the ratio between the NO_3 production rate via Reaction (R2) with rate coefficient k_2 and the mixing ratios of O_3, NO_2 and NO_3 (Eq. 2).

$$k_{ss}^{NO_3} = \frac{k_2\,[O_3]\,[NO_2]}{[NO_3]} \tag{2}$$

Acquiring steady state can take several hours if the NO_3 lifetime is long, temperatures are low or NO_2 mixing ratios are high (Brown et al., 2003). In the NO3ISOP experiments, the NO_3 reactivities were generally high, and steady state is achieved within a few minutes of isoprene being injected into the chamber. However, NO_2 reinjections in the chamber during periods of low reactivity at the end of an experiment when isoprene was already depleted can lead to a temporary breakdown of the steady-state assumption. In order to circumvent this potential source of error, the non-steady-state reactivities ($k_{nss}^{NO_3}$) based on NO_3 and N_2O_5 measurements (McLaren et al., 2010) were calculated using Eq. (3).

$$k_{nss}^{NO_3} = \frac{k_2\,[O_3]\,[NO_2] - \frac{d[NO_3]}{dt} - \frac{d[N_2O_5]}{dt}}{[NO_3]} \tag{3}$$

This expression is similar to Eq. (2) except for the subtraction of the derivatives $d[NO_3]/dt$ and $d[N_2O_5]/dt$ from the production term. A comparison of $k_{ss}^{NO_3}$ and $k_{nss}^{NO_3}$ is given in the Supplement and verifies the assumptions above: as soon as isoprene is injected into the system, $k_{ss}^{NO_3}$ and $k_{nss}^{NO_3}$ are equivalent (see Fig. S3a), but $k_{ss}^{NO_3}$ shows short-term deviations at NO_2 reinjections (see Fig. S3b). As the non-steady-state reactivities are less affected by such events, the latter were used for the comparison with the measured NO_3 reactivities. The steady-state and the non-steady-state calculations are only valid if equilibrium between NO_3 and N_2O_5 is established. Moreover, the N_2O_5 measurements are usually less sensitive to instrument-specific losses under dry conditions. For this reason, measured NO_3 mixing ratios were checked for consistency with the equilibrium to N_2O_5 using the equilibrium constant K_{eq} for Reactions (R3)/(R4) as well as the measured N_2O_5 and NO_2 mixing ratios as denoted in Eq. (4) for this analysis. In the case when a significant deviation was observed, NO_3 mixing ratios from $[NO_2]$, $[N_2O_5]$ and K_{eq} were used.

$$[NO_3]_{eq} = \frac{[N_2O_5]}{K_{eq}[NO_2]} \tag{4}$$

A time series of measured k^{NO_3} and calculated $k_{nss}^{NO_3}$ is depicted in Fig. 7a, which shows the results from experiments in the absence of aerosol only. It is evident that $k_{nss}^{NO_3}$ is much higher than k^{NO_3}. In Fig. 7b we plot k^{NO_3} versus $k_{nss}^{NO_3}$: an unweighted, orthogonal, linear fit has a slope of 0.54 ± 0.01 and indicates that the measured values of k^{NO_3} are almost a factor of 2 lower than $k_{nss}^{NO_3}$. Propagation of the uncertainties in k_2 (15 %; IUPAC, 2020) and the NO_3, NO_2 and O_3 mixing ratios (25 %, 9 % and 5 %, respectively) results in an overall uncertainty of 31 % for $k_{nss}^{NO_3}$, which cannot account for its deviation to k^{NO_3}.

The fact that $k_{nss}^{NO_3}$ is significantly larger than k^{NO_3} indicates that NO_3 can be lost by reactions other than those with reactive, stable VOCs that can be sampled by the FT-CRDS instrument. As discussed above, RO_2 represents the most likely candidate to account for some additional loss of NO_3; the numerical simulations (MCM v3.3.1) predict an additional reactivity of the order of ~ 22 % based on a generic value for $k_{NO_3+RO_2}$. However, in order to bring k^{NO_3} and $k_{nss}^{NO_3}$ into agreement, either the RO_2 level or the rate coefficient for reaction between NO_3 and RO_2 (especially

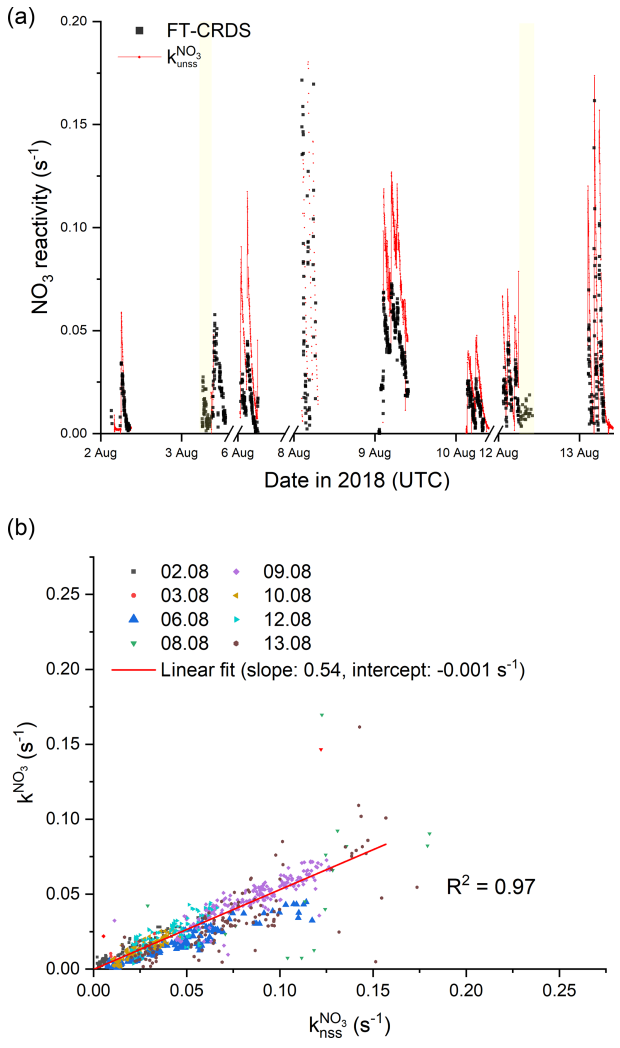

Figure 7. (a) Overview of measured (black) and calculated NO_3 reactivity with Eq. (3) (red). The ticks mark 00:00 UTC of the corresponding day. The yellow areas denote periods with an opened chamber roof. For the sake of clarity, the uncertainties are not included. **(b)** Correlation plot between k^{NO_3} and $k^{NO_3}_{nss}$. The red line represents an unweighted, orthogonal linear regression ($R^2 = 0.97$) of the complete data set.

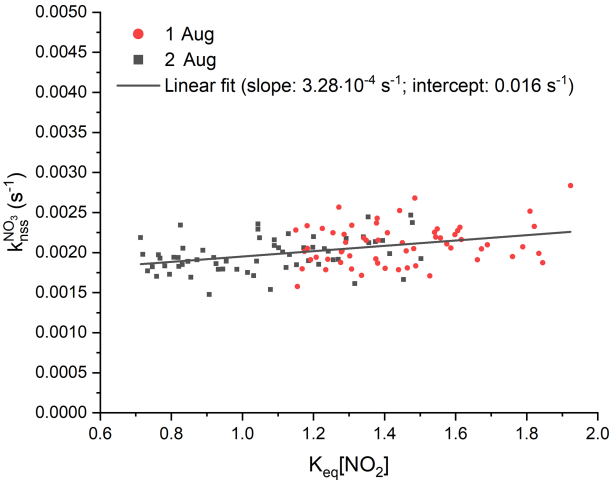

Figure 8. Analysis of the contribution of wall losses of NO_3 and N_2O_5 to NO_3 reactivity, $k^{NO_3}_{nss}$, are using experimental data during isoprene-free periods on the 1 August (red) and 2 August (black). Least-squares linear fit of the data is shown with a black line and yielded to an intercept $k^{NO_3}_{wall}$ of 0.016 s^{-1} and to a slope $k^{N_2O_5}_{wall}$ of 3.28×10^{-4} s^{-1}. For the sake of better clarity, error bars are not included.

NISOPOO) would have to be a factor of 2 larger than incorporated into the model (see below). Alternatively, losses of NO_3 (and N_2O_5) to surfaces enhance $k^{NO_3}_{nss}$ but not k^{NO_3}. As no aerosol was present in the experiments analysed above, the only surface available is provided by the chamber walls.

In order to quantify the contribution of NO_3 and N_2O_5 wall losses to $k^{NO_3}_{nss}$, we analysed the experiments from the 1 and 2 August during isoprene-free periods, i.e. when no RO_2 radicals are present and (in the absence of photolysis and NO) uptake of NO_3 (or N_2O_5) to the chamber walls represents the only significant sink. Consequently, plotting $k^{NO_3}_{nss}$ from this period against $K_{eq}[NO_2]$ enables separation of direct NO_3 losses (Reaction R10) from indirect losses via N_2O_5 uptake (Reaction R9) and to derive first-order loss rates ($k^{wall}_{NO_3}$ and $k^{wall}_{N_2O_5}$) of NO_3 and N_2O_5 according to Eq. (5) (Allan et al., 2000; Brown et al., 2009b; Crowley et al., 2010; McLaren et al., 2010).

$$k^{NO_3}_{nss} = k^{NO_3}_{wall} + k^{N_2O_5}_{wall} K_{eq}[NO_2] \quad (5)$$

The results from the isoprene-free periods of experiments on the 1 and 2 August are shown in Fig. 8. A linear regression of the data yields a slope ($k^{N_2O_5}_{wall}$) of $(3.28 \pm 1.15) \times 10^{-4}$ s^{-1} and an intercept ($k^{NO_3}_{wall}$) of (0.0016 ± 0.0001) s^{-1}, indicating that NO_3 losses dominate and that heterogeneous removal of N_2O_5 does not contribute significantly to the overall loss rate constant of ~ 0.002 s^{-1}. The data reproducibility from one experiment to the next indicates that the NO_3/N_2O_5 wall loss rates are unchanged if the experimental conditions, i.e. dry air and no aerosols, are comparable. Humidification of the air, on the other hand, may facilitate heterogeneous reactions of NO_3 or N_2O_5 with the chamber walls and increase corresponding loss rates. This might be an explanation for observation of a larger difference between k^{NO_3} and $k^{NO_3}_{nss}$ during an experiment under humid conditions on the 6 August (Fig. 7b, blue triangles). Lack of extensive isoprene-free periods on this day impede the extraction of wall loss rates with this approach: even after subtraction of k^{NO_3} from $k^{NO_3}_{nss}$, Eq. (5) is not applicable in experiments once isoprene is present (and becomes the dominant sink of NO_3) as reactions of RO_2 indirectly co-determine the NO_2 mixing ratios.

For further analysis, the wall loss rate constants of NO_3 and N_2O_5 were fixed as long as there was neither humidity nor particles in the chamber, and they are considered in-

variant with time after isoprene injections. This implicitly assumes that low-volatility oxidation products that deposit on chamber walls do not enhance the reactivity of the walls to NO_3. As these products have less double bonds than isoprene and react only very slowly with NO_3, this assumption would appear reasonable.

We examined the effect of introducing the NO_3 and N_2O_5 wall loss rate constants calculated as described above into the chemical scheme used in the box model (MCM v3.3.1). The results from three different model outputs for the experiment on the 2 August are summarized in Fig. 9, which compares simulated and measured mixing ratios of NO_3, N_2O_5, NO_2, O_3 and isoprene (following its addition at 11:00 UTC) as well as the measured and non-steady-state NO_3 reactivities k^{NO_3} and $k_{nss}^{NO_3}$. The omission of NO_3/N_2O_5 wall losses (model 1) results in simulated NO_3 and N_2O_5 mixing ratios up to 1400 and 1600 pptv, respectively, during the isoprene-free period, which exceed measurements by factors of 4–8. This is because the only loss process for these species in this phase is the dilution rate that is 2 orders of magnitude lower than the estimated wall loss rates. Such high amounts of NO_3/N_2O_5 in the parts per billion range result in rapid depletion of nearly half of the total injected isoprene within the first minute, which is why model 1 cannot describe the measurements either before or after the injection. Model 2 (red lines) includes the estimated wall loss rates and reproduces the measurements more accurately: the NO_2 and O_3 mixing ratios are accurately simulated. Furthermore, NO_3 and N_2O_5 mixing ratios that are only 10 % to 30 % higher than those measured and therefore NO_3 reactivities lower than $k_{nss}^{NO_3}$ (orange circles) are predicted.

The evolution of the isoprene mixing ratio is reproduced by the model, which is why k^{NO_3} (mostly determined by k_5[isoprene], purple area) is only slightly lower than the simulated overall reactivity by model 2. After quantification of NO_3/N_2O_5 wall losses, NO_3+RO_2 reactions remain the only source of additional NO_3 reactivity to explain the difference between k^{NO_3} and $k_{nss}^{NO_3}$. As already mentioned above, the model may underestimate the effect of RO_2-induced losses of NO_3 either because the RO_2 mixing ratios are underestimated or because the rate coefficient $k_{RO_2+NO_3}$ is larger than assumed.

The result of a simulation (model 3) with $k_{RO_2+NO_3}$ set to 4.6×10^{-12} cm^3 molecule^{-1} s^{-1} (twice the generic value in MCM v3.3.1) is displayed as the blue lines in Fig. 9. The O_3, NO_2, N_2O_5 and isoprene mixing ratios are only slightly affected by this change in the reaction constant, whereas its impact on the NO_3 mixing ratios as well as on the reactivity is very significant. The higher rate coefficient for reaction of NO_3 with RO_2 would be sufficient for the observed discrepancy between the overall reactivity $k_{nss}^{NO_3}$ and k^{NO_3} within the uncertainties associated with the analysis. Optimum agreement irrespective of uncertainties would be achieved with a value of 9.2×10^{-12} cm^3 molecule^{-1} s^{-1} for $k_{RO_2+NO_3}$ (i.e. a factor of 4 higher than in MCM), which is demonstrated in a comparable experiment under dry conditions on the 10 August (see Fig. S4 in the Supplement).

There are only few experimental studies on reactions of NO_3 with RO_2, and the rate coefficient for reaction of NO_3 with isoprene-derived RO_2 has never been measured. For the reaction between NO_3 and the methyl peroxy radical (CH_3O_2), values between 1.0×10^{-12} and 2.3×10^{-12} cm^3 molecule^{-1} s^{-1} have been reported (Crowley et al., 1990; Biggs et al., 1994; Daele et al., 1995; Helleis et al., 1996; Vaughan et al., 2006), with a preferred value of 1.2×10^{-12} cm^3 molecule^{-1} s^{-1} (Atkinson et al., 2006). Increasing the length of the C−C backbone in the peroxy radical appears to increase the rate coefficient, with values of 2.3×10^{-12} cm^3 molecule^{-1} s^{-1} preferred for reaction of NO_3 with $C_2H_5O_2$ (Atkinson et al., 2006), whereas the presence of electron-withdrawing groups attached to the peroxy carbon atom reduces the rate coefficient (Vaughan et al., 2006). A single study of the reaction between NO_3 and an acylperoxy radical indicates that the rate coefficient (4.0×10^{-12} cm^3 molecule^{-1} s^{-1}) may be larger than the MCM adopted value of 2.3×10^{-12} cm^3 molecule^{-1} s^{-1} (Canosa-Mas et al., 1996). Similarly, an indirect study (Hjorth et al., 1990) of the rate coefficient for the reaction between NO_3 and a nitro-substituted C_6 peroxy radical ($(CH_3)_2C(ONO_2)C(CH_3)_2O_2$) reports a value of 5×10^{-12} cm^3 molecule^{-1} s^{-1}, which may be appropriate for longer-chain peroxy radicals derived from biogenic trace gases. In light of the large uncertainty associated with the kinetics of $RO_2 + NO_3$ reactions, a rate coefficient of 4.6×10^{-12} cm^3 molecule^{-1} s^{-1} for reaction between NISOPOO and NO_3 is certainly plausible.

We note, however, that use of a faster rate coefficient for the reaction between RO_2 and NISOPOO, RO_2 isomerization processes and differentiation between the fates of the main NISOPOO isomers as proposed by Schwantes et al. (2015) would result in lower RO_2 mixing ratios. If $k_{NISOPOO+RO_2}$ in MCM v3.3.1 is set to a value of 5×10^{-12} cm^3 molecule^{-1} s^{-1} (average over all isomers, Schwantes et al., 2015), a slightly higher value of 5.2×10^{-12} cm^3 molecule^{-1} s^{-1} for $k_{RO_2+NO_3}$ would be necessary to bring modelled and measured NO_3 reactivity into agreement within associated uncertainties. Conversely, increasing RO_2 concentrations by the required factor of 2 would necessitate a significant reduction in the model rate coefficients for $RO_2 + RO_2$ or $RO_2 + HO_2$ reactions, which contradicts experimental results (Boyd et al., 2003; Schwantes et al., 2015) and is considered unlikely.

Differences in measurement of $k_{nss}^{NO_3}$ and modelled NO_3 reactivity could also result from incorrectly modelled product yields, owing to the simplified mechanism used, which, for example, does not consider in detail the formation of methyl vinyl ketone (MVK) via β-NISOPOO isomers or the reaction between NO_3 and other main products like hydroxy isopropyl nitrates (e.g. $O_2NOCH_2C(CH_3)CHCH_2OH$, ISOPCNO3) and nitrooxy

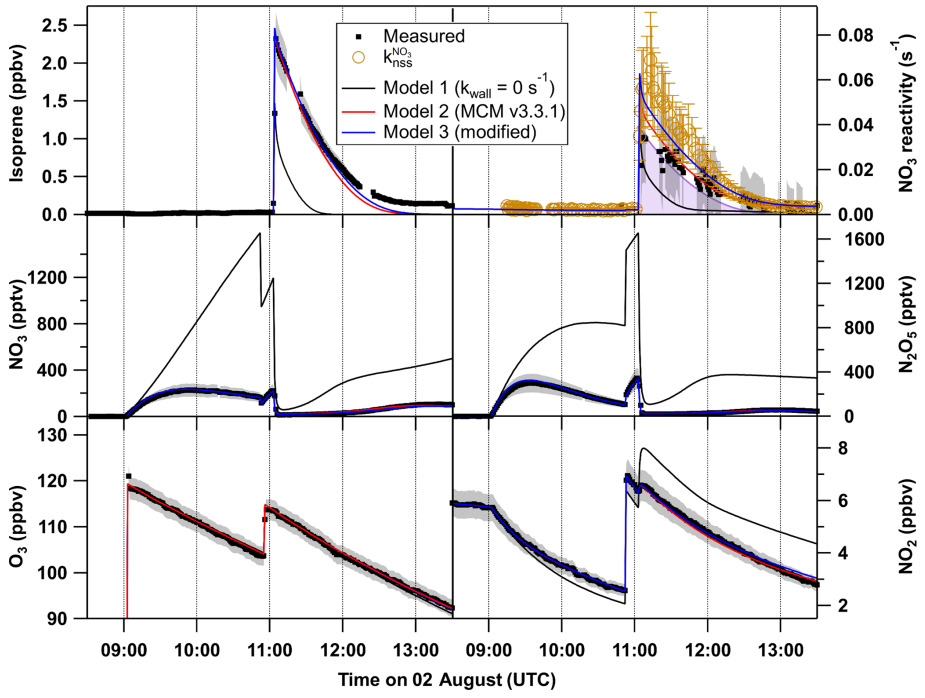

Figure 9. O_3, NO_2, NO_3, N_2O_5 and isoprene mixing ratios and NO_3 reactivity on 2 August (black). The grey shaded area symbolizes the overall uncertainty associated with each measurement. Orange circles denote the reactivity obtained using Eq. (3). The results of the numerical simulation using MCM v.3.3.1 with NO_3 and N_2O_5 wall loss rates set to $0\,s^{-1}$ (model 1) are shown by black lines. The model output with introduction of NO_3 and N_2O_5 wall loss rates of $0.016\,s^{-1}$ and $3.3 \times 10^{-4}\,s^{-1}$, respectively, for each of the reactants is shown by a red line (model 2), whereas the blue line (model 3) shows the result of model 2 with the rate coefficient for reaction between NO_3 and RO_2 set to 4.6×10^{-12} cm^3 molecule^{-1} s^{-1}, which is twice the value estimated by the MCM.

isopropyl hydroperoxide ($O_2NOCH_2C(CH_3)CHCH_2OOH$, NISOPOOH). However, none of these products is expected to react sufficiently rapidly with NO_3 to make a difference: the rate coefficient for reaction of NO_3 with MVK is $< 6 \times 10^{-16}$ cm^3 molecule^{-1} s^{-1} and that for 2-methyl-3-butene-2-ol (a comparable molecule to ISOPCNO3) is 1.2×10^{-14} cm^3 molecule^{-1} s^{-1} at 298 K (IUPAC, 2020). Even parts per billion amounts of these products would not cause significant additional NO_3 reactivity.

On the other hand, the FT-CRDS will underestimate the reactivity of NO_3 if products that are formed do not make it to the inlet (i.e. traces gases with high affinity for surfaces). One potential candidate for this category is NISOPOOH, formed in the reaction between NISOPOO and HO_2. There are no kinetic data on the reaction of NO_3 with NISOPOOH, though given the lack of reactivity of NO_3 towards organic peroxides it is very unlikely that the rate coefficient would be larger than for $NO_3 + O_2NOCH_2C(CH_3)$=CHCHO. Analysis of one experiment (9 August, Fig. 7b), in which HO_2 production (and thus the yield of NISOPOOH) was enhanced by the addition of propene and CO, shows that the difference between k^{NO_3} and $k_{nss}^{NO_3}$ on that day is comparable to those of the other experiments. This would also indicate that the influence of the potential non-detection of the hydroperoxide on the analysis should be low.

All in all, the results of the analysis above strongly suggest that the difference between directly measured and non-steady-state reactivity $k_{nss}^{NO_3}$ is caused by reactions of NO_3 with RO_2 with the results best explained when a rate coefficient of $\sim 5 \times 10^{-12}$ cm^3 molecule^{-1} s^{-1} is used. Quantifying the impact of peroxy radicals on the fate of NO_3, however, is challenging. The rate coefficients for $RO_2 + NO_3$ are scarce and uncertain and the rate constants for self-reaction of RO_2 derived from NO_3 + isoprene have not been determined in direct kinetic measurement but via analyses of non-radical product yields.

4 Summary and conclusion

Direct measurements of NO_3 reactivity (k^{NO_3}) in chamber experiments exploring the NO_3-induced oxidation of isoprene showed excellent agreement with NO_3 loss rate constants calculated from isoprene mixing ratios, thus underlining the reliability of the reactivity measurements even under unfavourable conditions with as much as 25 ppbv of NO_2 in the chamber. The main contributor to the overall uncertainty in k^{NO_3} is the correction (via numerical simulation) for the reaction of NO_3 with NO_2 and the thermal decomposition of the N_2O_5 product. The results of the NO3ISOP campaign

indicate that previously derived overall uncertainties (Liebmann et al., 2017) that considered an uncertainty of 10 % in the rate coefficients of both reactions (Burkholder et al., 2015) and an 8 % uncertainty for the NO_2 mixing ratios are too large.

The measured reactivity, k^{NO_3}, could be completely assigned to the reaction between NO_3 and isoprene, indicating that contributions from reactions of non-radical oxidation products are minor, which is consistent with predictions of the current version of the Master Chemical Mechanism.

Values of NO_3 reactivity as calculated from NO_3 and N_2O_5 mixing ratios and the NO_3 production term were found to be a factor of ~ 1.85 higher than the directly measured NO_3 reactivities (k^{NO_3}). A box model analysis indicates that the most likely explanation is a larger fractional loss of NO_3 via reactions with organic peroxy radicals (RO_2) formed during the oxidation of isoprene. A rate coefficient ($k_{RO_2+NO_3} = \sim 5 \times 10^{-12}$ cm^3 molecule^{-1} s^{-1}) is necessary to align model predictions (MCM v.3.3.1) and observations within associated uncertainties.

Data availability. The data from the experiments in the SAPHIR chamber used in this work are available on the EUROCHAMP data home page (https://data.eurochamp.org/data-access/chamber-experiments/, EUROCHAMP, 2020).

Supplement. The supplement related to this article is available online at: https://doi.org/10.5194/acp-20-10459-2020-supplement.

Author contributions. HF, AN and SSB designed and conducted the chamber experiments. PD, JML and JaS were responsible for the NO_3 reactivity measurements. CC and AN were responsible for the OH reactivity measurements. JuS, JNC, FB, LZ, SSB and WM were responsible for the NO_3 and N_2O_5 measurements and its evaluation. KX, RH, RT and DR were responsible for the PTR-MS measurements of VOCs. PD, NF, JML and JuS took and evaluated NO_2 and NO_x data. FR was responsible for O_3 and NO measurements. PD did the analysis and, with the help of JNC, wrote the paper. JL, HF, SSB, AN, CC, JML, FB, RH, KX and RT contributed to the article.

Competing interests. The authors declare that they have no conflict of interest.

Special issue statement. This article is part of the special issue "Simulation chambers as tools in atmospheric research (AMT/ACP/GMD inter-journal SI)". It is not associated with a conference.

Acknowledgements. We thank Chemours for provision of the FEP sample used to coat the cavities and flow tube reactor of the NO_3 reactivity setup.

Financial support. This research has been supported by Horizon 2020 (EUROCHAMP-2020 (grant no. 730997) and SARLEP (grant no. 681529)) and French National Research Agency/Labex VOLTAIRE (grant no. ANR-10-LABX-100-01).

The article processing charges for this open-access publication were covered by the Max Planck Society.

Review statement. This paper was edited by Thomas Karl and reviewed by two anonymous referees.

References

Allan, B. J., McFiggans, G., Plane, J. M. C., Coe, H., and McFadyen, G. G.: The nitrate radical in the remote marine boundary layer, J. Geophys. Res.-Atmos., 105, 24191–24204, 2000.

Atkinson, R. and Arey, J.: Gas-phase tropospheric chemistry of biogenic volatile organic compounds: a review, Atmos. Environ., 37, S197–S219, 2003.

Atkinson, R., Baulch, D. L., Cox, R. A., Crowley, J. N., Hampson, R. F., Hynes, R. G., Jenkin, M. E., Rossi, M. J., Troe, J., and IUPAC Subcommittee: Evaluated kinetic and photochemical data for atmospheric chemistry: Volume II – gas phase reactions of organic species, Atmos. Chem. Phys., 6, 3625–4055, https://doi.org/10.5194/acp-6-3625-2006, 2006.

Biggs, P., Canosa-Mas, C. E., Fracheboud, J.-M., Shallcross, D. E., and Wayne, R. P.: Investigation into the kinetics and mechanism of the reaction of NO_3 with CH_3O_2 at 298 K and 2.5 Torr: a potential source of OH in the night-time troposphere?, J. Chem. Soc., Faraday Trans., F90, 1205–1210, https://doi.org/10.1039/FT9949001205, 1994.

Bossmeyer, J., Brauers, T., Richter, C., Rohrer, F., Wegener, R., and Wahner, A.: Simulation chamber studies on the NO_3 chemistry of atmospheric aldehydes, Geophys. Res. Lett., 33, L18810, https://doi.org/10.1029/2006GL026778, 2006.

Boyd, A. A., Flaud, P. M., Daugey, N., and Lesclaux, R.: Rate constants for $RO_2 + HO_2$ reactions measured under a large excess of HO_2, J. Phys. Chem. A, 107, 818–821, 2003.

Brown, S. S. and Stutz, J.: Nighttime radical observations and chemistry, Chem. Soc. Rev., 41, 6405–6447, 2012.

Brown, S. S., Stark, H., and Ravishankara, A. R.: Applicability of the steady state approximation to the interpretation of atmospheric observations of NO_3 and N_2O_5, J. Geophys. Res.-Atmos., 108, 4539, https://doi.org/10.1029/2003JD003407, 2003.

Brown, S. S., Dibb, J. E., Stark, H., Aldener, M., Vozella, M., Whitlow, S., Williams, E. J., Lerner, B. M., Jakoubek, R., Middlebrook, A. M., DeGouw, J. A., Warneke, C., Goldan, P. D., Kuster, W. C., Angevine, W. M., Sueper, D. T., Quinn, P. K., Bates, T. S., Meagher, J. F., Fehsenfeld, F. C., and Ravishankara, A. R.: Nighttime removal of NO_x in the sum-

mer marine boundary layer, Geophys. Res. Lett., 31, L07108, https://doi.org/10.1029/2004GL019412, 2004.

Brown, S. S., Ryerson, T. B., Wollny, A. G., Brock, C. A., Peltier, R., Sullivan, A. P., Weber, R. J., Dube, W. P., Trainer, M., Meagher, J. F., Fehsenfeld, F. C., and Ravishankara, A. R.: Variability in nocturnal nitrogen oxide processing and its role in regional air quality, Science, 311, 67–70, 2006.

Brown, S. S., deGouw, J. A., Warneke, C., Ryerson, T. B., Dubé, W. P., Atlas, E., Weber, R. J., Peltier, R. E., Neuman, J. A., Roberts, J. M., Swanson, A., Flocke, F., McKeen, S. A., Brioude, J., Sommariva, R., Trainer, M., Fehsenfeld, F. C., and Ravishankara, A. R.: Nocturnal isoprene oxidation over the Northeast United States in summer and its impact on reactive nitrogen partitioning and secondary organic aerosol, Atmos. Chem. Phys., 9, 3027–3042, https://doi.org/10.5194/acp-9-3027-2009, 2009a.

Brown, S. S., Dube, W. P., Fuchs, H., Ryerson, T. B., Wollny, A. G., Brock, C. A., Bahreini, R., Middlebrook, A. M., Neuman, J. A., Atlas, E., Roberts, J. M., Osthoff, H. D., Trainer, M., Fehsenfeld, F. C., and Ravishankara, A. R.: Reactive uptake coefficients for N_2O_5 determined from aircraft measurements during the Second Texas Air Quality Study: Comparison to current model parameterizations, J. Geophys. Res.-Atmos., 114, D00F10, https://doi.org/10.1029/2008JD011679, 2009b.

Burkholder, J. B., Sander, S. P., Abbatt, J., Barker, J. R., Huie, R. E., Kolb, C. E., Kurylo, M. J., Orkin, V. L., Wilmouth, D. M., and Wine, P. H.: Chemical Kinetics and Photochemical Data for Use in Atmospheric Studies, Evaluation No. 18, JPL Publication 15-10, Jet Propulsion Laboratory, Pasadena, available at: http://jpldataeval.jpl.nasa.gov (last access: 7 September 2020), 2015.

Canosa-Mas, C. E., King, M. D., Lopez, R., Percival, C. J., Wayne, R. P., Shallcross, D. E., Pyle, J. A., and Daele, V.: Is the reaction between $CH_3C(O)O_2$ and NO_3 important in the night-time troposphere?, J. Chem. Soc., Faraday Trans., 92, 2211–2222, 1996.

Crowley, J. N., Burrows, J. P., Moortgat, G. K., Poulet, G., and LeBras, G.: Room temperature rate coefficient for the reaction between CH_3O_2 and NO_3, Int. J. Chem. Kinet., 22, 673–681, 1990.

Crowley, J. N., Schuster, G., Pouvesle, N., Parchatka, U., Fischer, H., Bonn, B., Bingemer, H., and Lelieveld, J.: Nocturnal nitrogen oxides at a rural mountain-site in south-western Germany, Atmos. Chem. Phys., 10, 2795–2812, https://doi.org/10.5194/acp-10-2795-2010, 2010.

Crowley, J. N., Thieser, J., Tang, M. J., Schuster, G., Bozem, H., Beygi, Z. H., Fischer, H., Diesch, J.-M., Drewnick, F., Borrmann, S., Song, W., Yassaa, N., Williams, J., Pöhler, D., Platt, U., and Lelieveld, J.: Variable lifetimes and loss mechanisms for NO_3 and N_2O_5 during the DOMINO campaign: contrasts between marine, urban and continental air, Atmos. Chem. Phys., 11, 10853–10870, https://doi.org/10.5194/acp-11-10853-2011, 2011.

Curtis, A. R. and Sweetenham, W. P.: Facsimile, Atomic Energy Research Establishment, Report R-12805, Harwell Laboratory, Oxfordshire, UK, 1987.

Daele, V., Laverdet, G., Lebras, G., and Poulet, G.: Kinetics of the reactions CH_3O+NO, CH_3O+NO_3, and $CH_3O_2+NO_3$, J. Phys. Chem., 99, 1470–1477, https://doi.org/10.1021/j100005a017, 1995.

Dorn, H.-P., Apodaca, R. L., Ball, S. M., Brauers, T., Brown, S. S., Crowley, J. N., Dubé, W. P., Fuchs, H., Häseler, R., Heitmann, U., Jones, R. L., Kiendler-Scharr, A., Labazan, I., Langridge, J. M., Meinen, J., Mentel, T. F., Platt, U., Pöhler, D., Rohrer, F., Ruth, A. A., Schlosser, E., Schuster, G., Shillings, A. J. L., Simpson, W. R., Thieser, J., Tillmann, R., Varma, R., Venables, D. S., and Wahner, A.: Intercomparison of NO_3 radical detection instruments in the atmosphere simulation chamber SAPHIR, Atmos. Meas. Tech., 6, 1111–1140, https://doi.org/10.5194/amt-6-1111-2013, 2013.

Dubé, W. P., Brown, S. S., Osthoff, H. D., Nunley, M. R., Ciciora, S. J., Paris, M. W., McLaughlin, R. J., and Ravishankara, A. R.: Aircraft instrument for simultaneous, in situ measurement of NO_3 and N_2O_5 via pulsed cavity ring-down spectroscopy, Rev. Sci. Instrum., 77, 034101, https://doi.org/10.1063/1.2176058, 2006.

Edwards, P. M., Aikin, K. C., Dube, W. P., Fry, J. L., Gilman, J. B., de Gouw, J. A., Graus, M. G., Hanisco, T. F., Holloway, J., Huber, G., Kaiser, J., Keutsch, F. N., Lerner, B. M., Neuman, J. A., Parrish, D. D., Peischl, J., Pollack, I. B., Ravishankara, A. R., Roberts, J. M., Ryerson, T. B., Trainer, M., Veres, P. R., Wolfe, G. M., Warneke, C., and Brown, S. S.: Transition from high- to low-NO_x control of night-time oxidation in the southeastern US, Nat. Geosci., 10, 490–495, https://doi.org/10.1038/Ngeo2976, 2017.

EUROCHAMP: Database of Atmospheric Simulation Chamber Studies, available at: https://data.eurochamp.org/data-access/chamber-experiments/, last accesss: 8 September 2020.

Fry, J. L., Brown, S. S., Middlebrook, A. M., Edwards, P. M., Campuzano-Jost, P., Day, D. A., Jimenez, J. L., Allen, H. M., Ryerson, T. B., Pollack, I., Graus, M., Warneke, C., de Gouw, J. A., Brock, C. A., Gilman, J., Lerner, B. M., Dubé, W. P., Liao, J., and Welti, A.: Secondary organic aerosol (SOA) yields from NO_3 radical + isoprene based on nighttime aircraft power plant plume transects, Atmos. Chem. Phys., 18, 11663–11682, https://doi.org/10.5194/acp-18-11663-2018, 2018.

Fuchs, H., Dube, W. P., Cicioira, S. J., and Brown, S. S.: Determination of inlet transmission and conversion efficiencies for in situ measurements of the nocturnal nitrogen oxides, NO_3, N_2O_5 and NO_2, via pulsed cavity ring-down spectroscopy, Anal. Chem., 80, 6010–6017, 2008.

Fuchs, H., Ball, S. M., Bohn, B., Brauers, T., Cohen, R. C., Dorn, H.-P., Dubé, W. P., Fry, J. L., Häseler, R., Heitmann, U., Jones, R. L., Kleffmann, J., Mentel, T. F., Müsgen, P., Rohrer, F., Rollins, A. W., Ruth, A. A., Kiendler-Scharr, A., Schlosser, E., Shillings, A. J. L., Tillmann, R., Varma, R. M., Venables, D. S., Villena Tapia, G., Wahner, A., Wegener, R., Wooldridge, P. J., and Brown, S. S.: Intercomparison of measurements of NO_2 concentrations in the atmosphere simulation chamber SAPHIR during the NO3Comp campaign, Atmos. Meas. Tech., 3, 21–37, https://doi.org/10.5194/amt-3-21-2010, 2010.

Fuchs, H., Simpson, W. R., Apodaca, R. L., Brauers, T., Cohen, R. C., Crowley, J. N., Dorn, H.-P., Dubé, W. P., Fry, J. L., Häseler, R., Kajii, Y., Kiendler-Scharr, A., Labazan, I., Matsumoto, J., Mentel, T. F., Nakashima, Y., Rohrer, F., Rollins, A. W., Schuster, G., Tillmann, R., Wahner, A., Wooldridge, P. J., and Brown, S. S.: Comparison of N_2O_5 mixing ratios during NO3Comp 2007 in SAPHIR, Atmos. Meas. Tech., 5, 2763–2777, https://doi.org/10.5194/amt-5-2763-2012, 2012.

Geyer, A. and Platt, U.: Temperature dependence of the NO_3 loss frequency: A new indicator for the contribution of NO_3 to the oxidation of monoterpenes and NO_x removal in the atmosphere, J. Geophys. Res.-Atmos., 107, 4431, https://doi.org/10.1029/2001JD001215, 2002.

Geyer, A., Alicke, B., Konrad, S., Schmitz, T., Stutz, J., and Platt, U.: Chemistry and oxidation capacity of the nitrate radical in the continental boundary layer near Berlin, J. Geophys. Res.-Atmos., 106, 8013–8025, 2001.

Guenther, A. B., Jiang, X., Heald, C. L., Sakulyanontvittaya, T., Duhl, T., Emmons, L. K., and Wang, X.: The Model of Emissions of Gases and Aerosols from Nature version 2.1 (MEGAN2.1): an extended and updated framework for modeling biogenic emissions, Geosci. Model Dev., 5, 1471–1492, https://doi.org/10.5194/gmd-5-1471-2012, 2012.

Heintz, F., Platt, U., Flentje, H., and Dubois, R.: Long-term observation of nitrate radicals at the tor station, Kap Arkona (Rugen), J. Geophys. Res.-Atmos., 101, 22891–22910, 1996.

Helleis, F., Moortgat, G. K., and Crowley, J. N.: Kinetic investigations of the reaction of CD_3O_2 with NO and NO_3 at 298 K, J. Phys. Chem., 100, 17846–17854, 1996.

Hjorth, J., Lohse, C., Nielsen, C. J., Skov, H., and Restelli, G.: Products and Mechanisms of the Gas-Phase Reactions between NO_3 and a Series of Alkenes, J. Phys. Chem., 94, 7494–7500, https://doi.org/10.1021/j100382a035, 1990.

Hohaus, T., Kuhn, U., Andres, S., Kaminski, M., Rohrer, F., Tillmann, R., Wahner, A., Wegener, R., Yu, Z., and Kiendler-Scharr, A.: A new plant chamber facility, PLUS, coupled to the atmosphere simulation chamber SAPHIR, Atmos. Meas. Tech., 9, 1247–1259, https://doi.org/10.5194/amt-9-1247-2016, 2016.

Holzinger, R.: PTRwid: A new widget tool for processing PTR-TOF-MS data, Atmos. Meas. Tech., 8, 3903–3922, https://doi.org/10.5194/amt-8-3903-2015, 2015.

Holzinger, R., Acton, W. J. F., Bloss, W. J., Breitenlechner, M., Crilley, L. R., Dusanter, S., Gonin, M., Gros, V., Keutsch, F. N., Kiendler-Scharr, A., Kramer, L. J., Krechmer, J. E., Languille, B., Locoge, N., Lopez-Hilfiker, F., Materić, D., Moreno, S., Nemitz, E., Quéléver, L. L. J., Sarda Esteve, R., Sauvage, S., Schallhart, S., Sommariva, R., Tillmann, R., Wedel, S., Worton, D. R., Xu, K., and Zaytsev, A.: Validity and limitations of simple reaction kinetics to calculate concentrations of organic compounds from ion counts in PTR-MS, Atmos. Meas. Tech., 12, 6193–6208, https://doi.org/10.5194/amt-12-6193-2019, 2019.

IUPAC: Task Group on Atmospheric Chemical Kinetic Data Evaluation, edited by: Ammann, M., Cox, R. A., Crowley, J. N., Herrmann, H., Jenkin, M. E., McNeill, V. F., Mellouki, A., Rossi, M. J., Troe, J., and Wallington, T. J., available at: http://iupac.pole-ether.fr/index.html, last access: 7 September 2020.

Jenkin, M. E., Young, J. C., and Rickard, A. R.: The MCM v3.3.1 degradation scheme for isoprene, Atmos. Chem. Phys., 15, 11433–11459, https://doi.org/10.5194/acp-15-11433-2015, 2015.

Khan, M. A. H., Cooke, M. C., Utembe, S. R., Archibald, A. T., Derwent, R. G., Xiao, P., Percival, C. J., Jenkin, M. E., Morris, W. C., and Shallcross, D. E.: Global modeling of the nitrate radical (NO_3) for present and pre-industrial scenarios, Atmos. Res., 164, 347–357, https://doi.org/10.1016/j.atmosres.2015.06.006, 2015.

Krechmer, J., Lopez-Hilfiker, F., Koss, A., Hutterli, M., Stoermer, C., Deming, B., Kimmel, J., Warneke, C., Holzinger, R., Jayne, J., Worsnop, D., Fuhrer, K., Gonin, M., and de Gouw, J.: Evaluation of a New Reagent-Ion Source and Focusing Ion-Molecule Reactor for Use in Proton-Transfer-Reaction Mass Spectrometry, Anal. Chem., 90, 12011–12018, https://doi.org/10.1021/acs.analchem.8b02641, 2018.

Lelieveld, J., Butler, T. M., Crowley, J. N., Dillon, T. J., Fischer, H., Ganzeveld, L., Harder, H., Lawrence, M. G., Martinez, M., Taraborrelli, D., and Williams, J.: Atmospheric oxidation capacity sustained by a tropical forest, Nature, 452, 737–740, 2008.

Lelieveld, J., Gromov, S., Pozzer, A., and Taraborrelli, D.: Global tropospheric hydroxyl distribution, budget and reactivity, Atmos. Chem. Phys., 16, 12477–12493, https://doi.org/10.5194/acp-16-12477-2016, 2016.

Liebmann, J. M., Schuster, G., Schuladen, J. B., Sobanski, N., Lelieveld, J., and Crowley, J. N.: Measurement of ambient NO3 reactivity: design, characterization and first deployment of a new instrument, Atmos. Meas. Tech., 10, 1241–1258, https://doi.org/10.5194/amt-10-1241-2017, 2017.

Liebmann, J., Karu, E., Sobanski, N., Schuladen, J., Ehn, M., Schallhart, S., Quéléver, L., Hellen, H., Hakola, H., Hoffmann, T., Williams, J., Fischer, H., Lelieveld, J., and Crowley, J. N.: Direct measurement of NO_3 radical reactivity in a boreal forest, Atmos. Chem. Phys., 18, 3799–3815, https://doi.org/10.5194/acp-18-3799-2018, 2018a.

Liebmann, J. M., Muller, J. B. A., Kubistin, D., Claude, A., Holla, R., Plass-Dülmer, C., Lelieveld, J., and Crowley, J. N.: Direct measurements of NO_3 reactivity in and above the boundary layer of a mountaintop site: identification of reactive trace gases and comparison with OH reactivity, Atmos. Chem. Phys., 18, 12045–12059, https://doi.org/10.5194/acp-18-12045-2018, 2018b.

Martinez, M., Perner, D., Hackenthal, E. M., Kulzer, S., and Schutz, L.: NO_3 at Helgoland during the NORDEX campaign in October 1996, J. Geophys. Res.-Atmos., 105, 22685–22695, 2000.

McLaren, R., Wojtal, P., Majonis, D., McCourt, J., Halla, J. D., and Brook, J.: NO_3 radical measurements in a polluted marine environment: links to ozone formation, Atmos. Chem. Phys., 10, 4187–4206, https://doi.org/10.5194/acp-10-4187-2010, 2010.

Mogensen, D., Gierens, R., Crowley, J. N., Keronen, P., Smolander, S., Sogachev, A., Nölscher, A. C., Zhou, L., Kulmala, M., Tang, M. J., Williams, J., and Boy, M.: Simulations of atmospheric OH, O_3 and NO_3 reactivities within and above the boreal forest, Atmos. Chem. Phys., 15, 3909–3932, https://doi.org/10.5194/acp-15-3909-2015, 2015.

Ng, N. L., Brown, S. S., Archibald, A. T., Atlas, E., Cohen, R. C., Crowley, J. N., Day, D. A., Donahue, N. M., Fry, J. L., Fuchs, H., Griffin, R. J., Guzman, M. I., Herrmann, H., Hodzic, A., Iinuma, Y., Jimenez, J. L., Kiendler-Scharr, A., Lee, B. H., Luecken, D. J., Mao, J., McLaren, R., Mutzel, A., Osthoff, H. D., Ouyang, B., Picquet-Varrault, B., Platt, U., Pye, H. O. T., Rudich, Y., Schwantes, R. H., Shiraiwa, M., Stutz, J., Thornton, J. A., Tilgner, A., Williams, B. J., and Zaveri, R. A.: Nitrate radicals and biogenic volatile organic compounds: oxidation, mechanisms, and organic aerosol, Atmos. Chem. Phys., 17, 2103–2162, https://doi.org/10.5194/acp-17-2103-2017, 2017.

Paulot, F., Henze, D. K., and Wennberg, P. O.: Impact of the isoprene photochemical cascade on tropical ozone, Atmos. Chem. Phys., 12, 1307–1325, https://doi.org/10.5194/acp-12-1307-2012, 2012.

Phillips, G. J., Thieser, J., Tang, M., Sobanski, N., Schuster, G., Fachinger, J., Drewnick, F., Borrmann, S., Bingemer, H., Lelieveld, J., and Crowley, J. N.: Estimating N_2O_5 uptake coefficients using ambient measurements of NO_3, N_2O_5, $ClNO_2$ and particle-phase nitrate, Atmos. Chem. Phys., 16, 13231–13249, https://doi.org/10.5194/acp-16-13231-2016, 2016.

Ridley, B. A., Grahek, F. E., and Walega, J. G.: A small, high-sensitivity, medium-response ozone detector suitable for measurements from light aircraft, J. Atmos. Ocean. Tech., 9, 142–148, 1992.

Rohrer, F., Bohn, B., Brauers, T., Brüning, D., Johnen, F.-J., Wahner, A., and Kleffmann, J.: Characterisation of the photolytic HONO-source in the atmosphere simulation chamber SAPHIR, Atmos. Chem. Phys., 5, 2189–2201, https://doi.org/10.5194/acp-5-2189-2005, 2005.

Rollins, A. W., Kiendler-Scharr, A., Fry, J. L., Brauers, T., Brown, S. S., Dorn, H.-P., Dubé, W. P., Fuchs, H., Mensah, A., Mentel, T. F., Rohrer, F., Tillmann, R., Wegener, R., Wooldridge, P. J., and Cohen, R. C.: Isoprene oxidation by nitrate radical: alkyl nitrate and secondary organic aerosol yields, Atmos. Chem. Phys., 9, 6685–6703, https://doi.org/10.5194/acp-9-6685-2009, 2009.

Saunders, S. M., Jenkin, M. E., Derwent, R. G., and Pilling, M. J.: Protocol for the development of the Master Chemical Mechanism, MCM v3 (Part A): tropospheric degradation of non-aromatic volatile organic compounds, Atmos. Chem. Phys., 3, 161–180, https://doi.org/10.5194/acp-3-161-2003, 2003.

Schwantes, R. H., Teng, A. P., Nguyen, T. B., Coggon, M. M., Crounse, J. D., St Clair, J. M., Zhang, X., Schilling, K. A., Seinfeld, J. H., and Wennberg, P. O.: Isoprene NO_3 Oxidation Products from the $RO_2 + HO_2$ Pathway, J. Phys. Chem. A, 119, 10158–10171, https://doi.org/10.1021/acs.jpca.5b06355, 2015.

Sharkey, T. D. and Yeh, S.: Isoprene emission from plants, Annu. Rev. Plant. Phys., 52, 407–436, https://doi.org/10.1146/annurev.arplant.52.1.407, 2001.

Sobanski, N., Schuladen, J., Schuster, G., Lelieveld, J., and Crowley, J. N.: A five-channel cavity ring-down spectrometer for the detection of NO_2, NO_3, N_2O_5, total peroxy nitrates and total alkyl nitrates, Atmos. Meas. Tech., 9, 5103–5118, https://doi.org/10.5194/amt-9-5103-2016, 2016a.

Sobanski, N., Tang, M. J., Thieser, J., Schuster, G., Pöhler, D., Fischer, H., Song, W., Sauvage, C., Williams, J., Fachinger, J., Berkes, F., Hoor, P., Platt, U., Lelieveld, J., and Crowley, J. N.: Chemical and meteorological influences on the lifetime of NO_3 at a semi-rural mountain site during PARADE, Atmos. Chem. Phys., 16, 4867–4883, https://doi.org/10.5194/acp-16-4867-2016, 2016b.

Thieser, J., Schuster, G., Schuladen, J., Phillips, G. J., Reiffs, A., Parchatka, U., Pöhler, D., Lelieveld, J., and Crowley, J. N.: A two-channel thermal dissociation cavity ring-down spectrometer for the detection of ambient NO_2, RO_2NO_2 and $RONO_2$, Atmos. Meas. Tech., 9, 553–576, https://doi.org/10.5194/amt-9-553-2016, 2016.

van Meeningen, Y., Schurgers, G., Rinnan, R., and Holst, T.: BVOC emissions from English oak (*Quercus robur*) and European beech (*Fagus sylvatica*) along a latitudinal gradient, Biogeosciences, 13, 6067–6080, https://doi.org/10.5194/bg-13-6067-2016, 2016.

Vaughan, S., Canosa-Mas, C. E., Pfrang, C., Shallcross, D. E., Watson, L., and Wayne, R. P.: Kinetic studies of reactions of the nitrate radical (NO_3) with peroxy radicals (RO_2): an indirect source of OH at night?, Phys. Chem. Chem. Phys., 8, 3749–3760, 2006.

Wagner, N. L., Dubé, W. P., Washenfelder, R. A., Young, C. J., Pollack, I. B., Ryerson, T. B., and Brown, S. S.: Diode laser-based cavity ring-down instrument for NO_3, N_2O_5, NO, NO_2 and O_3 from aircraft, Atmos. Meas. Tech., 4, 1227–1240, https://doi.org/10.5194/amt-4-1227-2011, 2011.

Warneke, C., de Gouw, J. A., Goldan, P. D., Kuster, W. C., Williams, E. J., Lerner, B. M., Jakoubek, R., Brown, S. S., Stark, H., Aldener, M., Ravishankara, A. R., Roberts, J. M., Marchewka, M., Bertman, S., Sueper, D. T., McKeen, S. A., Meagher, J. F., and Fehsenfeld, F. C.: Comparison of daytime and nighttime oxidation of biogenic and anthropogenic VOCs along the New England coast in summer during New England Air Quality Study 2002, J. Geophys. Res.-Atmos., 109, D10309, https://doi.org/10.1029/2003JD004424, 2004.

Wayne, R. P., Barnes, I., Biggs, P., Burrows, J. P., Canosamas, C. E., Hjorth, J., Lebras, G., Moortgat, G. K., Perner, D., Poulet, G., Restelli, G., and Sidebottom, H.: The Nitrate Radical – Physics, Chemistry, and the Atmosphere, Atmos. Environ., 25, 1–203, 1991.

Wennberg, P. O., Bates, K. H., Crounse, J. D., Dodson, L. G., McVay, R. C., Mertens, L. A., Nguyen, T. B., Praske, E., Schwantes, R. H., Smarte, M. D., St Clair, J. M., Teng, A. P., Zhang, X., and Seinfeld, J. H.: Gas-Phase Reactions of Isoprene and Its Major Oxidation Products, Chem. Rev., 118, 3337–3390, https://doi.org/10.1021/acs.chemrev.7b00439, 2018.